Petroleum Science 20 (2023) 141–160

Contents lists available at ScienceDirect

Petroleum Science

journal homepage: www.keaipublishing.com/en/journals/petroleum-science

Original Paper

Differences in geochemistry and hydrocarbon generation of source-rock samples dominated by telalginite and lamalginite: A case study on the Permian saline lacustrine source rocks in the Jimusaer Sag, NW China

Shi-Ju Liu [a, b], Gang Gao [a, b, *], Wen-Zhe Gang [a, b], Bao-Li Xiang [c], Ming Wang [c]

[a] College of Geosciences, China University of Petroleum, No. 18 Fuxue Road, Beijing, 102249, China
[b] State Key Laboratory of Petroleum Resource and Prospecting, China University of Petroleum, No. 18 Fuxue Road, Beijing, 102249, China
[c] Experimental Testing Institute, PetroChina Xinjiang Oilfield Company, Karamay, Xinjiang, 834000, China

ARTICLE INFO

Article history:
Received 11 March 2022
Received in revised form
12 April 2022
Accepted 30 August 2022
Available online 17 September 2022

Edited by Teng Zhu and Jia-Jia Fei

Keywords:
Maceral component
Biomarker compounds
Oil generation kinetics
Activation energy
Lucaogou formation

ABSTRACT

The Middle Permian Lucaogou Formation in Northwestern China mainly contains typical saline lacustrine oil shale. To study the differences in geochemistry and hydrocarbon generation of source-rock samples in Lucaogou Formation in Jimusaer Sag, 57 core samples from two boreholes were analyzed herein by performing total organic carbon (TOC) analysis, Rock–Eval pyrolysis, and gas chromatographic–mass spectrometry experiments on saturated hydrocarbons. The kinetics of oil generation were studied using two samples comprising typical maceral components. The results showed that the hydrocarbons produced by telalginite are relatively rich in pristane (Pr), phytane (Ph), β-carotane, high-carbon normal alkanes, and C_{29} regular steranes. Hydrocarbons produced by lamalginite contain a significantly higher content of C_{20} tricyclic terpanes (TT), C_{21}TT, C_{24} tetracyclic terpanes (TeT), C_{29} norhopane, and C_{28} regular sterane. Based on the pyrolysis and biomarker compound parameters, telalginite has a higher conversion rate for hydrocarbons than lamalginite in the low-mature to mature stage, which is consistent with their kinetic analysis. Lamalginite source rock displays a much narrower distribution of activation energies than telalginite source rocks. Such narrower activation energy distribution effectively narrows the main stage of hydrocarbon generation. In addition, the activation energy distribution of lamalginite concentrated in the high-value interval, indicating the characteristics of the relatively lagging hydrocarbon generation of lamalginite.

1. Introduction

According to traditional organic geochemistry theory, the formation of oil and gas is the process of thermal maturation of organic matter, which chemically degrades the macromolecules (kerogen) in the geologic body under thermodynamic interactions in geological history (Schaefer et al., 1990; Behar et al., 1992; Pepper and Corvi, 1995). Therefore, large-scale oil and gas accumulation often requires a substantial material basis of organic matter. Hydrocarbon generation from kerogen evolution is a process that invloves multistage organic chemical reactions (Burnham and Sweeney, 1989; Domine et al., 1998; Schenk and Horsfield, 1998; Dieckmann et al., 2006; Erdmann and Horsfield, 2006; Mahlstedt et al., 2008). As for the dynamic mechanism of different types of kerogens that evolve for the generation of hydrocarbons, the opinions vary among scholars (Huang et al., 1984; Tissot et al., 1987; Quigley and Mackenzie, 1988). Tissot et al. (1987) believed that the activation energy of different types of kerogens required for the generation of hydrocarbons has a sequence of $E_{II} < E_I < E_{III}$ (E_I: activation energy of Type I kerogen). Some scholars believed that the time sequence for hydrocarbon generation by kerogen is as follows: Type I kerogen > Type II kerogen > Type III kerogen (Fu and Shi, 1975). The hydrocarbon generation characteristics of different types of kerogens are related to the hydrocarbon generation

* Corresponding author. College of Geosciences, China University of Petroleum, No. 18 Fuxue Road, Beijing, 102249, China.
E-mail address: gaogang2819@sina.com (G. Gao).

https://doi.org/10.1016/j.petsci.2022.08.034

activation energies of different samples. Although it is verified to be the same type of kerogen according to the hydrogen index (HI), its kinetics may change significantly (Peters et al., 2006) and it is generally believed that the activation energy of Type I kerogen is narrowly distributed and that of Type III kerogen is relatively wide and asymmetrical (Tegelaar and Noble, 1994; Petersen and Rosenberg, 2000). The source rocks of the same shale series will exhibit different biological composition characteristics. Moreover, only a part of the organisms actually participated in the generation of oil and gas. Thus, the organisms' capacity and properties required for the generation of hydrocarbons determine the degree of enrichment or the amount of oil and gas resources produced.

The Middle Permian Lucaogou Formation in Northern Xinjiang contains the typical lacustrine Type I–II_1 kerogen, with a high abundance of organic matter (Gao et al., 2016; Cao et al., 2017; Luo et al., 2018); however, the source rock has been in the low-mature stage (Luo et al., 2018), thereby generating limited hydrocarbons. Based on organic petrology, Hackley et al. (2016) and Liu et al. (2017) classified hydrocarbon-generating parent materials in source rocks into two primary types: telalginite and lamalginite. In previous studies, the telalginite and lamalginite have different biological origins. For the telalginite, genera identified to date are mostly derived from planktonic *Chlorophyceae*, such as *Botryococcus* (Tissot and Welte, 1984; Sherwood, 1991), *Tasmanitids* (Saxby, 1980) and *Gloeocapsomorpha* (Sherwood, 1991). Marine sediments typically contain at least some Dinoflagellate and Acritarch-derived lamalginite, such as the Toarcian shale of Europe (Prauss et al., 1991). Lamalginite of lacustrine origin are the *Pediastrum* (Rundle, Queensland, Australia; Saxby, 1980; Hutton, 1982; Lindner, 1983) and *Cyanophyceae* (Green River Formation, USA; Sherwood, 1991; Tissot and Welte, 1984). Hackley et al. (2016) and Liu et al. (2022) believed that the biological sources of the telalginite and lamalginite in the Lucaogou Formation is Green algae and *Cyanobacteria*, respectively. This study aims to investigate the hydrocarbon generation kinetics of typical source rock samples containing lamalginite and telalginite from the Lucaogou Formation in the Jimusaer Sag and compares the hydrocarbon generation characteristics of different hydrocarbon-generating parent materials. The results provide some guidance that is significant for the identification of the source and the hydrocarbon generation of source rocks formed in saline environments.

2. Geological setting

The Jimusaer Sag, located in the southeastern part of the Junggar Basin, is a failed rift showing the shape of a dustpan with faults on its west and overlapped strata on its east. Peripherally, this sag is connected to the Beisantai Uplift in the west, Guxi Uplift in the east, Qitai Uplift in the north, and Fukang Fault in the south, covering an area of approximately 1278 km^2 (Fig. 1a) via the boundary controlled by the Jimusaer Fault trending north, Laozhuangwan Fault trending west, and Xidi and Santai Faults trending south (Yi, 2018). The strata from the Carboniferous to the Quaternary are sequentially deposited in the Jimusaer Sag, upwardly including the Carboniferous, the Permian Wutong and Jingjingzigou Formations, the Triassic, the Jurassic, the Cretaceous, the Paleogene, the Neogene, and the Quaternary (Fig. 1b). Miscellaneous facies deposits, including coastal shallow lacustrine, shallow lacustrine–semi-deep lacustrine, semi-deep lacustrine–deep lacustrine facies, and delta front facies, developed in the Lucaogou Formation in the Jimusaer Sag (Fang et al., 2005; Yi, 2018). Upwardly, the Lucaogou Formation is longitudinally divided into two sweet-spot bodies located in the upper and lower members (Cao et al., 2016, 2017). The oil and gas in the upper and lower sweet-spot bodies originate from the source rocks of the upper and lower members of the Lucaogou Formation, respectively (Gao et al., 2016; Bai et al., 2017). This study mainly focused on the source rocks in the upper member of the Lucaogou Formation.

3. Samples and methodology

3.1. Sample descriptions

A total of 29 and 28 shale samples were obtained from Wells A and JY74, respectively. Details of these samples are provided in Table 1. All the samples were analyzed using total organic carbon content (TOC) analysis, Rock–Eval pyrolysis, and gas chromatography–mass spectrometry (GC–MS).

3.2. TOC analysis and Rock–Eval pyrolysis

The TOC analysis of rock powder samples was performed using a Leco CS-230 carbon analyzer. Rock– Eval pyrolysis was performed using an OGE-II rock pyrolyzer developed by the Experimental Center of Petroleum Geology of the Research Institute of PetroChina Exploration and Development for obtaining parameters such as S_1 (mg, hydrocarbon (HC)/g rock), S_2 (mg HC/g rock) and T_{max} (°C).

3.3. GC–MS

Source rock powder (< 100 mesh) samples were extracted using chloroform in a Soxhlet apparatus and placed in a water bath (80 °C) for 48 h. The soluble extracts (bitumen) were then obtained after the evaporation of solvents in the airing chamber at room temperature. Fraction separation of the soluble extracts was conducted via conventional column chromatography. The extracts were dissolved in excess petroleum ether for 24 h, and then an insoluble component (asphaltene) was obtained by filtering. The saturated hydrocarbons, aromatic hydrocarbons, and resins in soluble residues were eluted with *n*-hexane, toluene, and the mixture of toluene and methanol (vol:vol = 1:1), respectively. The saturated hydrocarbon fractions were analyzed using an Agilent 7890-5975C GC and MS. Helium (purity of 99.999%) was introduced as the carrier gas with an injection port temperature of 300 °C and transmission-line temperature of 300 °C. The GC equipment is equipped with a fused silica capillary column (30 m×0.25 mm coated with a silica gel film having a thickness of 0.25 μm. During the experiment, the GC oven was programmed to hold at 50 °C for 1 min, to increase to 200 °C at a rate of 20 °C/min, to increase to 250 °C at a rate of 4 °C/min, to increase to 300 °C at a rate of 3 °C/min, and hold for 30 min. The flow rate of the carrier gas was set at 1 mL/min. The mass spectrometer was operated in the electron ionization mode at a voltage of 1047 V.

3.4. Organic petrographic

According to the ICCP (1998), ICCP (2001) and Pickel et al. (2017), the liptinite, vitrinite, and intertinite group macerals were identified. The lamaginite and telalginite are the major macerals in liptinite. The lamalginite usually appears as distinguish thin lamellae of alginite from larger, more strongly fluorescing, apparently continuous layers comprise numerous, small discontinuous

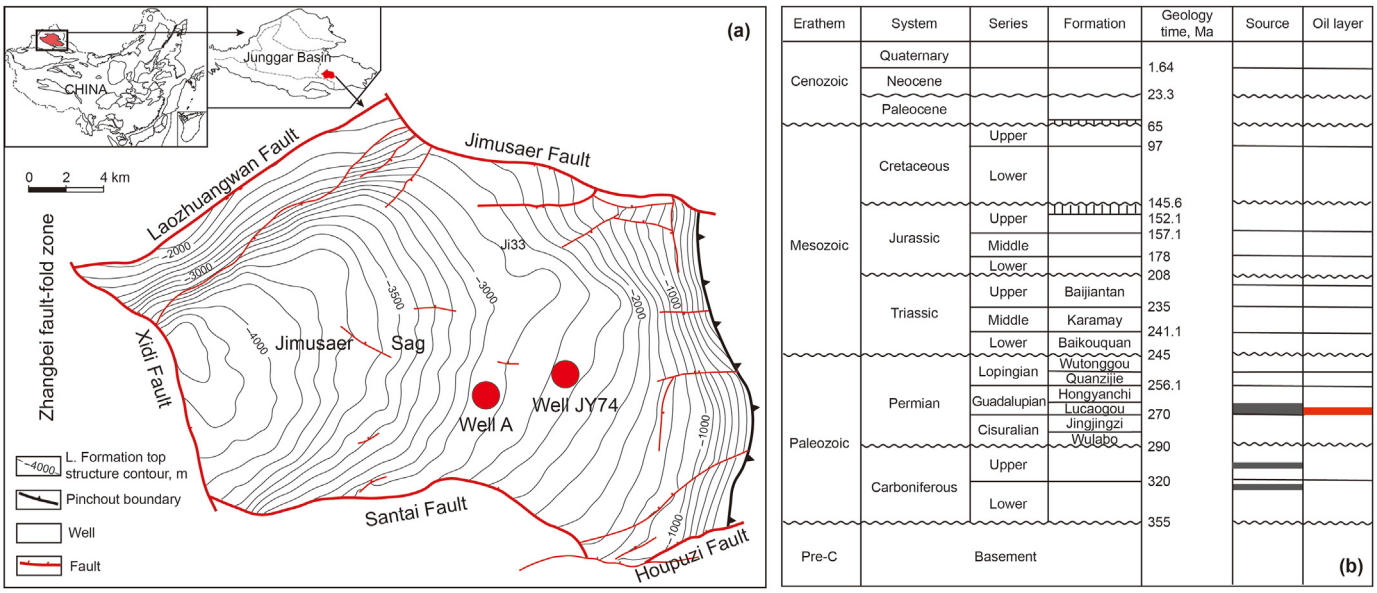

Fig. 1. Location and generalized stratigraphy of the Jimusaer Sag. (**a**): Locations of source rock sampling wells in the Jimusaer Sag, Junggar Basin. (**b**) Stratigraphy of the Jimusaer Sag (modified from Gao et al., 2016).

lamellae. In sections perpendicular to bedding, little structure is generally evident (Hutton, 1987). While the telalginite is the alginite that occurs as discrete lenses, fan-shaped masses or flattened discs all of which have distinctive external form and, in most cases, internal structure. As observed in this paper, the characteristics of telalginite in sections perpendicular to bedding are as follows: distributed discretely in lenticular form (Fig. 2a, and b), and the middle part of the individual algal showed red-orange fluorescence and the edge fluorescence was yellow (Fig. 2a, and b). Moreover, photoshop image processing software was then used to process the photos under fluorescent and reflected light (50 and above respectively, so that different locations of the entire sample could be covered) to determine the percentages of different substances in the sample.

3.5. Kinetic analysis

Two typical samples were selected from the upper member of the Lucaogou Formation in Well A. The basic geochemical information of these two samples is shown in Tables 1 and 2. From the perspective of organic matter abundance, the TOC in sample SR-1 was 6.19% and the value of pyrolysis parameters S_1, S_2, and T_{max} was 1.99 mg HC/g rock, 40.36 mg HC/g rock, and 445 °C, respectively (Table 1). Correspondingly, the TOC in sample SR-2 was 25.1%, which was higher than that in sample SR-1, and the value of S_1, S_2, and T_{max} of 1.41 mg HC/g rock, 195.82 mg HC/g rock, and 452 °C, respectively (Table 1). The HI values of the two samples (SR-1: 652 and SR-2: 780.2) indicated the dominance of Type I kerogen in the source rocks. Petrographic analysis revealed that the organic matter in sample SR-1 is dominated by telalginite (Fig. 2a and c and Table 2), which shows characteristics similar to that of chlorophyta with an orangish-red fluorescence in the middle and bright yellow illumination in the surrounding (Fig. 2a) (Hackley et al., 2016). However, the organic matter of sample SR-2 mainly comprised lamalginite with extremely good stratification. Scanning electron microscope observations suggest that lamalginite is superimposed in a sheet distribution (Fig. 2f). Furthermore, vitrinite, semifilament, and fungus can also be found in the two samples (Fig. 2b and e). The maturity of the source rock reflected by samples SR-1 and SR-2 is in a relatively low-mature stage, showing vitrinite reflectance of 0.77% and 0.77% on an average, respectively (Table 2 and Fig. 3).

Herein, different rates of the constant-heating method were used to obtain the hydrocarbon-generation conversion rate-temperature curve under different heating conditions. Detailed experimental steps are as follows: (1) four parallel samples of ~100 mg were prepared from each sample, and the analytical cycle of the Rock–Eval instrument was set for performing activation energy analysis. Specifically, the sample was set to be heated at a constant temperature of 200 °C for 5 min to remove adsorbed hydrocarbons and was then heated from 200 °C to 600 °C at a constant rate in different stages. (2) Real-time records of the product quantity and hydrocarbon-generation conversion rate were collected under different conditions. According to the data recorded, the temperature versus hydrocarbon rate curve was mapped to calibrate the kinetic parameters during hydrocarbon generation. For these two samples, a heating rate scheme of 20 °C/min, 30 °C/min, 40 °C/min, and 50 °C/min was adopted. In the kinetic analysis, the energy interval of the discrete activation energy distribution of parallel reactions is 1.0 kJ/mol, which corresponds to an optimized frequency factor (Wang et al., 2011).

4. Results

4.1. Rock–Eval, TOC and maceral data

Basic geochemical information obtained from TOC analysis and Rock–Eval pyrolysis are shown in Tables 1 and 3, respectively. The TOC values varies between 1.25 wt%–30.10 wt% (mean = 6.64 wt%). The Rock–Eval S_1 and S_2 values vary between 0.02 and 4.04 (mean = 0.94 mg HC/g rock) and 1.20–202.56 mg HC/g rock (mean = 44.00 mg HC/g rock), respectively (Table 3). The TOC and S_2 values indicated that the organic matter in the Lucaogou Formation is characterized by I-II_1 type and high organic matter

Table 1
Origin and bulk properties of the studied source rock samples from upper member of Lucaogou Formation in Jimusaer Sag.

Well No.	Samples	Depth, m	TOC, %	T_{max}, °C	S_1, mg HC/g rock	S_2, mg HC/g rock	HI, mg HC/g TOC	HCI, mg HC/g TOC	EOM, %	EOM/TOC
A	**SR-1***	**3518.25**	**6.19**	**445**	**1.99**	**40.36**	**652**	**32.15**	**0.96**	**15.57**
A	**SR-2***	**3577.1**	**25.1**	**452**	**1.41**	**195.82**	**780.2**	**5.62**	**0.21**	**0.82**
A	A-1	3499.54	8.38	444	3.07	46.81	558.59	36.63	0.99	11.84
A	A-2	3501.74	4.04	445	1.5	20.62	510.4	37.13	0.42	10.43
A	A-3	3503.71	2.85	445	0.45	9.68	339.65	15.79	0.17	5.88
A	A-4*	3506.31	1.86	448	0.38	6.65	357.53	20.43	0.11	6.1
A	A-5	3512.72	6.61	447	2.51	38.43	581.39	37.97	0.83	12.56
A	A-6*	3515.35	7.76	444	2.95	48.99	631.31	38.02	0.9	11.58
A	A-7*	3516.05	5.31	441	2.89	28.77	541.81	54.43	1.02	19.26
A	A-8*	3517.35	5.76	445	1.55	33.86	587.85	26.91	0.82	14.28
A	A-9*	3521.03	8.75	440	4.04	42.81	489.26	46.17	0.96	10.96
A	A-10*	3523.78	6.66	444	1.21	42.7	641.14	18.17	0.77	11.55
A	A-11	3525.87	12.2	444	1.62	82.54	676.56	13.28	0.38	3.09
A	A-12	3530.54	9.82	449	1.1	71.77	730.86	11.2	0.3	3.07
A	A-13	3531.09	24.7	449	2.13	202.56	820.08	8.62	0.32	1.29
A	A-14*	3532.79	6.37	446	0.71	52.38	822.29	11.15	0.11	1.74
A	A-15	3546.17	7.09	448	3.13	47.49	669.82	44.15	1.19	16.8
A	A-16	3548.28	6.42	449	0.7	47.14	734.27	10.9	0.38	5.94
A	A-17*	3554.51	4.07	445	0.65	26.91	661.18	15.97	0.18	4.33
A	A-18	3561.85	4.29	449	0.54	27.4	638.69	12.59	0.1	2.23
A	A-19*	3567.50	30.1	457	1.49	188.1	624.92	4.95	0.19	0.63
A	A-20*	3569.20	5.22	449	0.41	40.19	769.92	7.85	0.13	2.55
A	A-21*	3571.60	2.33	442	0.66	9.19	394.42	28.33	0.26	11.36
A	A-22*	3582.10	12.9	450	1.21	100.49	778.99	9.38	0.3	2.32
A	A-23*	3586.20	7.8	448	0.78	64.17	822.69	10	0.1	1.34
A	A-24*	3592.45	1.25	447	0.09	5.88	470.4	7.2	0.04	3.26
A	A-25*	3595.40	6.06	447	2.01	40.66	670.96	33.17	0.46	7.6
A	A-26*	3597.10	4.12	449	0.72	27.43	665.78	17.48	0.37	8.9
A	A-27*	3600.50	6.01	448	0.77	39.79	662.06	12.81	0.22	3.65
JY74	JY-1	3110.88	3.55	448	0.66	8.35	235.21	18.59	0.37	10.48
JY74	JY-2	3114.73	1.42	451	0.28	3.87	272.54	19.72	0.11	7.71
JY74	JY-3	3117.75	5.57	449	0.53	22.48	403.59	9.52	0.14	2.47
JY74	JY-4	3118.78	9.77	453	0.44	78.96	808.19	4.50	0.12	1.27
JY74	JY-5	3119.23	13.9	451	0.34	97.31	700.07	2.45	2.59	18.61
JY74	JY-6	3122.14	2.84	448	0.49	8.85	311.62	17.25	0.16	5.55
JY74	JY-7	3122.58	3.96	450	0.33	17.32	437.37	8.33	0.13	3.20
JY74	JY-8	3130.76	3.03	445	0.4	4.16	137.29	13.20	0.05	1.67
JY74	JY-9	3134.05	6.77	444	0.74	32.75	483.75	10.93	0.50	7.40
JY74	JY-10	3134.21	6.05	448	0.88	22.19	366.78	14.55	0.59	9.74
JY74	JY-11	3137.01	6.25	452	0.36	32.9	526.4	5.76	0.17	2.69
JY74	JY-12	3145.44	3.73	452	0.47	24.99	669.97	12.60	0.19	5.05
JY74	JY-13	3146.16	2.72	441	0.79	6.98	256.62	29.04	0.44	16.01
JY74	JY-14	3146.19	1.88	445	0.25	3.11	165.43	13.30	0.18	9.41
JY74	JY-15	3150.2	2.48	448	0.64	3.2	129.03	25.81	0.17	6.67
JY74	JY-16	3152.82	3.17	451	0.02	20.2	637.22	0.63	1.01	31.72
JY74	JY-17	3152.98	13.86	454	0.59	152.17	1097.91	4.26	0.22	1.60
JY74	JY-18	3153.65	2.14	453	0.12	1.2	56.07	5.61	0.06	2.63
JY74	JY-19	3155.32	12.42	452	0.65	176	1417.07	5.23	0.12	0.99
JY74	JY-20	3156.94	2.32	453	0.15	4.32	186.21	6.47	0.10	4.28
JY74	JY-21	3158.88	2.54	444	0.24	12.95	509.84	9.45	0.08	3.20
JY74	JY-22	3161.75	1.85	448	0.02	10.85	586.49	1.08	0.39	21.01
JY74	JY-23	3162.02	3.22	453	0.17	10.76	334.16	5.28	0.14	4.27
JY74	JY-24	3165.87	8.19	455	0.48	49.23	601.1	5.86	0.31	3.75
JY74	JY-25	3169.19	4.03	455	0.28	16.96	420.84	6.95	0.14	3.44
JY74	JY-26	3171.29	3.65	446	0.3	27.38	750.14	8.22	0.10	2.62
JY74	JY-27	3177.55	3.9	448	0.26	21.37	547.95	6.67	0.15	3.95
JY74	JY-28	3177.57	3.39	455	0.21	7.8	230.09	6.19	0.15	4.28

abundance; however, the low S_1 values indicated that the source rock in the Lucaogou Formation was at a relatively low thermal maturity stage. The extracted organic matter (EOM) and EOM/TOC varied from 0.04% to 2.59% (mean = 0.39%) and from 0.63% to 31.72% (mean = 7.13%), respectively (Table 3). HI (S_2/TOC×100) and Hydrocarbon Index (HCI: S_1/TOC×100) values ranged 56.07–1417.07 (mean = 553.75 mg HC/g TOC) and 0.63–53.43 mg HC/g TOC (mean = 15.89 mg HC/g TOC), respectively (Table 3). There are considerable variations in the HI, HCI, and EOM/TOC, indicating heterogeneity in the organic matter composition in the Lucaogou Formation source rocks.

The maceral percentages are showed in Table 2. The Liptinite in Lucaogou Formation include lamalginite, telalginite and mineral bituminous groundmass (MBG). Lamalginite (2 to 93 vol%, avg. 42 vol%), telalginite (0 to 83 vol%, avg. 40 vol%) and MBG (mineral bituminous groundmass) (2 to 22 vol%, avg. 10 vol%) occur in high

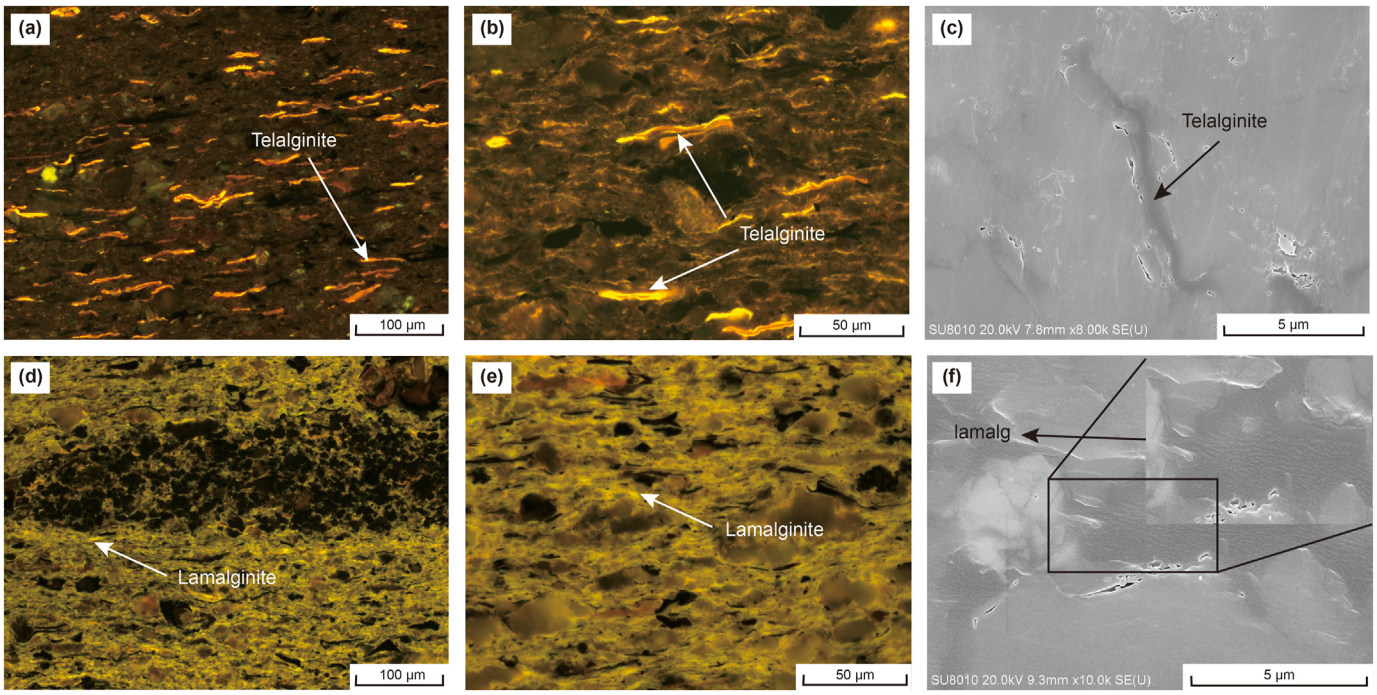

Fig. 2. Photographs of typical maceral. The observed samples were all along the vertical bedding plane. (**a**), (**b**), (**d**) and (**e**) are taken under oil immersion. (**a**): brightly fluorescent tel. with orange color under fluorescent light use 20×lens (SR-1); (**b**): brightly fluorescent tel. with orange color under fluorescent light use 50×lens (SR-1); (**c**): SEM image of tel. fossils (SR-1); (**d**): brightly fluorescent lamalginite with green yellow color under fluorescent light use 20×lens (SR-2); (**e**): brightly fluorescent lamalginite with green yellow color under fluorescent light use 50×lens (SR-2); (**f**): SEM image of lamalginite fossils (SR-2).

Table 2
Macerals and vitrinite reflectance data of the source rock samples from upper member of Lucaogou Formation in Well A in Jimusaer Sag.

Sampes	Depth, m	Lipt., vol%, mmf			Vitr., vol%, mmf	Inert., vol%, mmf	R_o, %
		telalginite	lamalginite	MBG			
SR-1[a]	3518.25	80	2	3	6	10	0.77
SR-2[a]	3577.1	Tr	93	Tr	1	6	0.77
A-4[a]	3506.31	62	4	10	7	17	
A-6[a]	3515.35	67	4	11	8	10	
A-7[a]	3516.05	83	2	2	7	6	
A-8[a]	3517.35	60	12	13	9	6	0.76
A-9[a]	3521.03	72	2	6	10	10	
A-10[a]	3523.78	69	5	8	10	8	
A-14[a]	3532.79	44	43	Tr	6	7	
A-17[a]	3554.51	31	55	Tr	4	10	
A-18	3561.85	Tr	87	2	7	4	
A-19[a]	3567.50	Tr	77	Tr	10	13	0.74
A-20[a]	3569.20	12	73	Tr	3	12	
A-21[a]	3571.60	2	79	Tr	12	8	
A-22[a]	3582.10	17	59	Tr	10	14	
A-23[a]	3586.20	Tr	93	Tr	Tr	6	0.76
A-24[a]	3592.45	20	70	Tr	5	5	
A-25[a]	3595.40	3	71	Tr	10	15	
A-26[a]	3597.10	46	10	19	10	15	
A-27[a]	3600.50	48	11	22	9	11	0.78

[a] Data are from Liu et al. (2022); Tr: present in trace quantities.

percentages, whereas vitrinite (3 to 12 vol%, avg. 8 vol%) and intertinite (4 to 17 vol%, avg. 10 vol%) were observed in lower concentrations (Table 2).

4.2. Molecular composition of hydrocarbons

4.2.1. n-Alkanes and acyclic isoprenoids

The total ion chromatogram (TIC) and m/z = 125 spectra of saturated hydrocarbons for the SR-1 and SR-2 are displayed in Fig. 4. The *n*-alkane distribution of the samples represented a unimodal distribution in the nC_{14} to nC_{35} interval. Evident high abundance of β-carotane and hopane compounds can be observed in SR-1, showing the peak carbon numbers of *n*-alkane at nC_{25} (Fig. 4a and b). Sample SR-2 was characterized by lower content of hopane and β-carotane with the peak carbon numbers of *n*-alkanes at C_{21} (Fig. 4c and d). The ratios of Pr/Ph, Ph/nC_{18}, Pr/nC_{17}, nC_{20-}/nC_{21+}, β-carotane/nC_{max} in normal paraffins are presented in Table 4.

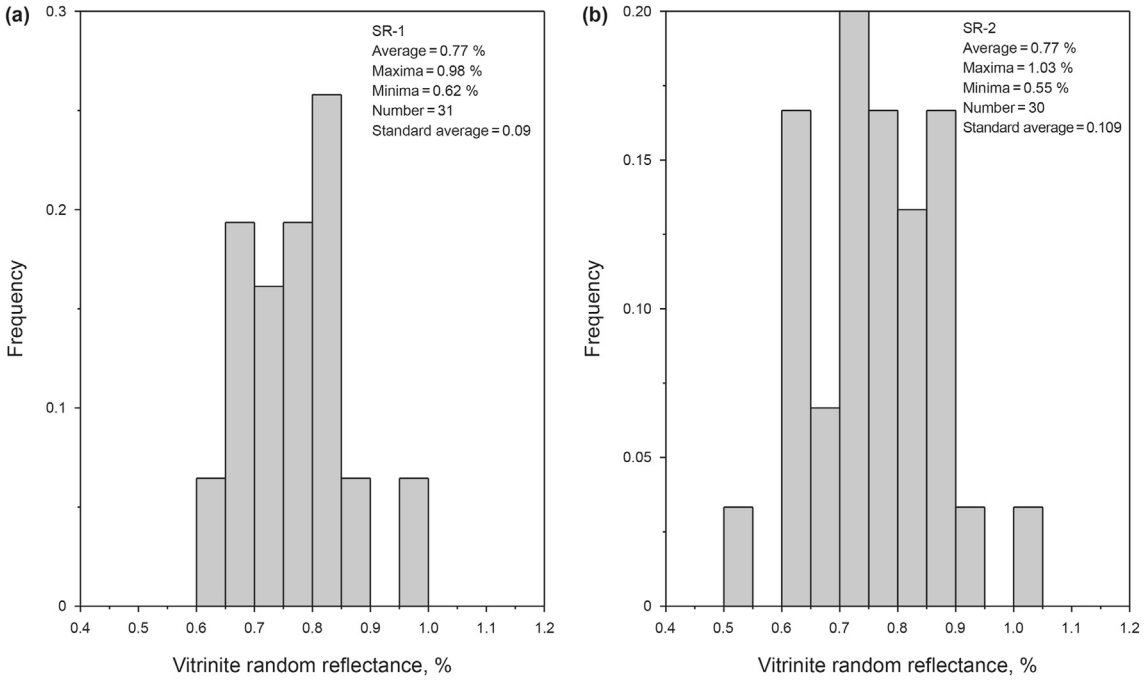

Fig. 3. Histogram of frequency distribution of vitrinite reflectance to reflects the maturity of the sample. (**a**):SR-1 sample; (**b**): SR-2 sample.

Table 3
Statistical data of the tested TOC, EOM contents and Rock-Eval parameters for the from upper member of Lucaogou Formation in Jimusaer Sag.

Index	Max	Min	Ave.
TOC, %	30.10	1.25	6.64
T_{max}, °C	457	440	448
S_1, mg HC/g rock	4.04	0.02	0.94
S_2, mg HC/g rock	202.56	1.20	44.00
HI, mg HC/g TOC	1417.07	56.07	553.75
HCI, mg HC/g TOC	54.43	0.63	15.89
EOM, %	2.59	0.04	0.39
EOM/TOC	31.72	0.63	7.13

4.2.2. Terpanes

Tricyclic terpanes (TTs) and C_{24}-tetracyclic terpane (TeT) can be clearly observed in sample SR-2 (Fig. 5) and are present in extremely low concentrations in SR-1 (Fig. 5). In the m/z = 191 spectrogram, the C_{27} and C_{29}–C_{34} hopanes can be clearly detected in both samples (Fig. 5). The content of C_{27}, 18α(H)-22,29,30 trisnorneohopane (Ts) and C_{30} diahopane in the two samples is extraordinarily low, indicating that the two types of macerals were developed in a clay-deficient environment (Peters et al., 2005). The biomarker parameters related to the samples, including C_{20}/C_{23}TT, C_{24}TeT/C_{26}TT, and C_{29}αβ/C_{30}αβ hopane ratio results, are shown in Table 4.

4.2.3. Steranes

The C_{21}–C_{22} pregnane and C_{27}–C_{29} regular sterane of the two samples are shown in Fig. 5. The results of the C_{28}/C_{29} regular sterane ratio of the two samples (SR-1:0.46, SR-2:1.21) indicate the difference in organic matter source for the two samples (Table 4) (Moldowan, 1985; Volkman and Maxwell, 1986). The C_{29} steranes ααα20S/(20S+20R) and ββ/(ββ+αα) ratios of sample SR-1 were 0.37 and 0.21, respectively, and those of sample SR-2 were 0.40 and 0.37, respectively (Table 4). Parameters of other biomarker compounds are listed in Table 4.

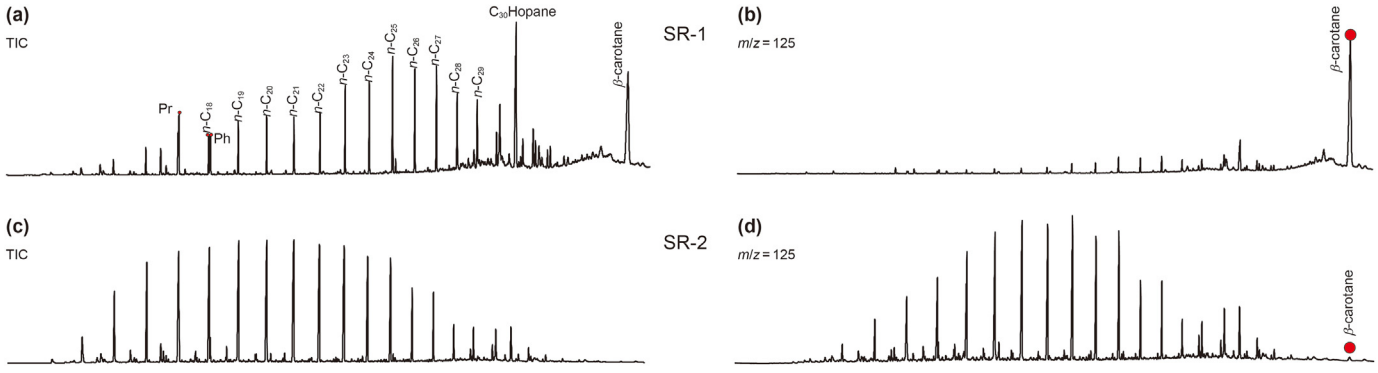

Fig. 4. Total ion chromatograms and m/z 125 mass chromatograms of the aliphatic fraction of extracts.

Table 4
Aliphatic hydrocarbon parameters for the studied samples from the Jimusaer Sag.

Well No.	Samples	TAR	$nC_{20}-/nC_{21}+$	Pr/Ph	Pr/nC_{17}	Ph/nC_{18}	β-carotane/nC_{max}	$C_{20}/C_{23}TT$	$C_{21}/C_{23}TT$	$C_{24}TeT/C_{26}TT$	$C_{29}\alpha\beta/C_{30}\alpha\beta$hopane	$C_{27}/C_{29}\alpha\alpha\alpha$20R sterane	$C_{28}/C_{29}\alpha\alpha\alpha$20R sterane	$C_{29}\alpha\alpha\alpha$20S/(20S+20R) sterane	C_{29} $\alpha\beta\beta/(\alpha\beta\beta+\alpha\alpha\alpha)$ sterane
A	**SR-1***	**1.15**	**0.49**	**1.30**	**1.62**	**1.28**	**1.84**	**0.81**	**1.04**	**1.34**	**0.30**	**0.68**	**0.46**	**0.37**	**0.21**
A	**SR-2***	**0.16**	**1.66**	**1.38**	**0.19**	**0.13**	**0.00**	**2.73**	**3.27**	**8.27**	**0.94**	**0.65**	**1.21**	**0.40**	**0.18**
A	A-1	0.68	0.73	1.29	1.67	1.43	0.16	0.33	1.85	0.68	0.22	0.29	0.45	0.41	0.34
A	A-2	1.38	0.46	1.61	2.33	1.43	0	0.39	1.62	1.69	0.28	0.23	0.66	0.4	0.32
A	A-3	1.38	0.52	1.13	0.57	0.41	0	0.48	2.43	2.14	0.31	0.59	0.69	0.43	0.33
A	A-4*	1.82	0.43	1.12	0.58	0.41	0.05	0.64	2.69	2.56	0.22	0.67	0.56	0.41	0.43
A	A-5	1.6	0.41	0.48	1.32	1.39	0	0.64	0.97	1.19	0.38	0.56	0.71	0.41	0.26
A	A-6[a]	1.35	0.47	0.8	0.98	1.13	0.26	0.64	1.65	1.42	0.27	0.57	0.64	0.4	0.25
A	A-7[a]	1.3	0.44	0.8	1.15	1.33	0.34	0.56	1.72	1.31	0.23	0.65	0.64	0.41	0.26
A	A-8[a]	0.69	0.98	1.44	1.71	1.39	3.62	0.85	1.08	1.36	0.27	0.79	0.51	0.39	0.23
A	A-9[a]	0.76	0.66	1.37	1.8	1.35	0.97	0.96	1.82	1.84	0.47	0.68	0.51	0.34	0.16
A	A-10[a]	1.26	0.47	1.14	1.5	1.11	0.21	1.14	1.22	2.76	0.36	0.86	0.6	0.37	0.18
A	A-11	0.89	0.57	0.87	1.27	1.4	0.39	0.56	1.24	1.15	0.26	0.58	0.73	0.41	0.29
A	A-12	/	1.42	1	0.68	0.62	0	1.32	1.4	4.03	0.39	0.8	0.93	0.44	0.28
A	A-13	0.49	0.94	1.15	0.63	0.61	0	1.71	1.56	4.62	0.41	0.77	0.93	0.4	0.22
A	A-14[a]	0.42	1.05	0.95	0.64	0.64	0.1	1.79	2.41	4.15	0.59	0.32	0.67	0.41	0.31
A	A-15	0.95	0.64	1.08	0.93	0.77	3.72	0.76	0.9	3.08	0.59	0.45	0.57	0.37	0.19
A	A-16	1.76	0.36	1	0.63	0.56	0	0.95	1.03	3.49	0.53	0.51	0.7	0.39	0.22
A	A-17[a]	1.04	0.61	0.97	0.46	0.42	0.03	1.71	3.08	5.41	0.58	0.33	0.89	0.4	0.25
A	A-18	0.53	1	1.17	1.23	1.37	0.93	1.87	1.21	14.77	0.97	0.86	1.58	0.45	0.23
A	A-19[a]	0.14	1.78	1.19	0.35	0.24	0	2.35	2.32	9.61	0.92	0.35	1.19	0.4	0.21
A	A-20[a]	0.21	1.39	1.1	0.3	0.21	0	1.69	2.19	7.82	0.92	0.28	0.94	0.37	0.2
A	A-21[a]	0.56	0.82	1.22	0.14	0.07	0	2.51	3.91	14.72	0.78	0.39	1.11	0.41	0.2
A	A-22[a]	0.26	0.94	0.88	0.39	0.3	0	1.36	1.26	5.68	0.8	0.22	0.71	0.38	0.18
A	A-23[a]	0.4	0.84	0.79	0.24	0.17	0	3.08	3.2	11.41	0.91	0.31	1.38	0.39	0.16
A	A-24[a]	4.56	0.31	0.5	0.33	0.2	0	1.19	2.02	6.11	0.49	0.4	0.9	0.42	0.25
A	A-25[a]	0.8	0.71	0.92	0.33	0.21	0	1.2	1.85	3.91	0.71	0.32	0.99	0.37	0.19
A	A-26*	0.75	0.76	1.22	0.67	0.55	0	1.29	1.27	3	0.45	0.83	0.73	0.39	0.21
A	A-27*	0.36	1.01	0.9	0.54	0.37	0.07	1.64	2.07	5.94	0.71	0.48	0.74	0.39	0.17
JY74	JY-1	1.12	0.53	1.08	2.67	2.43	1.58	0.65	0.91	2.29	0.50	0.29	0.65	0.32	0.23
JY74	JY-2	1.12	0.57	1.21	1.21	1.18	0.16	1.25	1.26	2.83	0.45	0.87	0.79	0.35	0.21
JY74	JY-3	0.10	1.86	1.23	0.84	0.85	0.22	1.79	1.68	3.94	0.47	0.48	0.75	0.39	0.24
JY74	JY-4	0.13	2.02	1.51	0.63	0.58	0.14	1.74	1.66	4.59	0.64	0.40	0.73	0.40	0.26
JY74	JY-5	0.50	0.87	1.18	0.90	0.80	0.35	1.20	1.39	2.50	0.63	0.33	0.67	0.43	0.35
JY74	JY-6	0.53	0.96	1.87	1.12	0.69	0.03	2.30	1.52	12.39	0.79	0.27	0.58	0.31	0.18
JY74	JY-7	0.40	1.01	1.69	1.50	1.04	0.22	1.43	1.30	8.32	0.81	0.25	0.84	0.33	0.20
JY74	JY-8	0.55	0.89	1.04	1.14	0.90	0.39	1.71	1.65	4.77	0.66	0.65	0.74	0.36	0.23
JY74	JY-9	0.71	0.59	1.42	1.89	1.73	0.67	1.23	1.25	3.11	0.62	0.52	0.75	0.31	0.19
JY74	JY-10	1.04	0.63	1.24	2.02	1.62	2.16	1.12	1.17	2.87	0.65	0.48	0.68	0.30	0.18
JY74	JY-11	0.98	0.58	1.52	1.41	1.03	0.76	1.14	1.05	3.19	0.78	0.50	0.87	0.29	0.17
JY74	JY-12	0.44	1.03	1.16	0.87	0.86	0.10	1.68	1.65	4.59	0.78	0.38	0.83	0.40	0.26
JY74	JY-13	0.63	0.70	1.29	0.54	0.38	0.02	1.09	1.06	3.60	0.70	0.42	1.08	0.30	0.18
JY74	JY-14	0.54	0.93	1.03	0.50	0.45	0.03	0.87	0.92	2.28	0.76	0.54	1.35	0.31	0.17
JY74	JY-15	0.93	0.63	1.93	0.34	0.14	0.00	2.46	1.65	7.69	1.08	0.66	1.14	0.31	0.17
JY74	JY-16	0.89	0.58	1.26	0.88	0.71	0.10	1.56	1.38	4.15	0.91	0.51	2.14	0.39	0.26
JY74	JY-17	0.21	1.49	1.40	0.62	0.51	0.03	2.53	1.87	9.13	0.99	0.47	1.96	0.36	0.23
JY74	JY-18	0.95	0.53	1.10	0.58	0.47	0.02	2.93	1.95	12.54	1.01	0.50	1.37	0.34	0.20
JY74	JY-19	0.10	1.88	2.10	0.20	0.09	0.00	3.14	1.84	20.89	1.19	0.54	2.38	0.29	0.19
JY74	JY-20	0.40	1.09	1.77	0.62	0.30	0.03	1.56	1.18	9.74	0.87	0.25	0.77	0.29	0.18
JY74	JY-21	0.50	0.92	1.21	0.14	0.09	0.00	2.17	1.50	21.57	0.88	0.50	1.07	0.31	0.19
JY74	JY-22	0.40	0.91	1.49	0.17	0.08	0.00	2.20	1.51	9.44	0.93	0.58	1.29	0.30	0.20
JY74	JY-23	0.37	0.99	1.46	0.15	0.08	0.00	1.96	1.45	17.63	0.93	0.49	1.16	0.30	0.18
JY74	JY-24	0.44	0.97	1.47	0.23	0.13	0.00	1.88	1.34	6.26	0.88	0.64	1.52	0.32	0.17
JY74	JY-25	0.93	0.58	1.17	0.48	0.36	0.00	2.18	1.38	5.72	0.88	0.41	1.05	0.35	0.19
JY74	JY-26	0.53	0.71	1.06	0.26	0.17	0.03	1.20	1.15	4.68	0.74	0.47	1.01	0.31	0.17
JY74	JY-27	1.12	0.49	1.07	0.25	0.22	0.00	1.42	1.17	7.67	0.71	0.55	1.00	0.37	0.21
JY74	JY-28	1.16	0.51	1.05	0.26	0.22	0.02	1.30	1.13	8.16	0.69	0.51	0.94	0.36	0.21

[a] Data are from Liu et al., (2022)..

4.3. Kinetic results

Data of cumulative hydrocarbon generation rate and temperature of samples SR-1 and SR-2 are provided in Tables 5 and 6. Among them, the activation energy of sample SR-1 had a wide distribution (110–420 kJ/mol, E_{AVE} = 259 kJ/mol); however, the activation energy of sample SR-2 was relatively concentrated in the range 255–300 kJ/mol (mean: 245 kJ/mol) (Table 7).

5. Discussion

5.1. Characteristics of typical biomarker compounds of source rocks intermediating SR-1 and SR-2

Pr and Ph are commonly used in geochemical research for identifying the source of organic matter and deciphering the environment in which it was deposited (Peters and Moldowan,

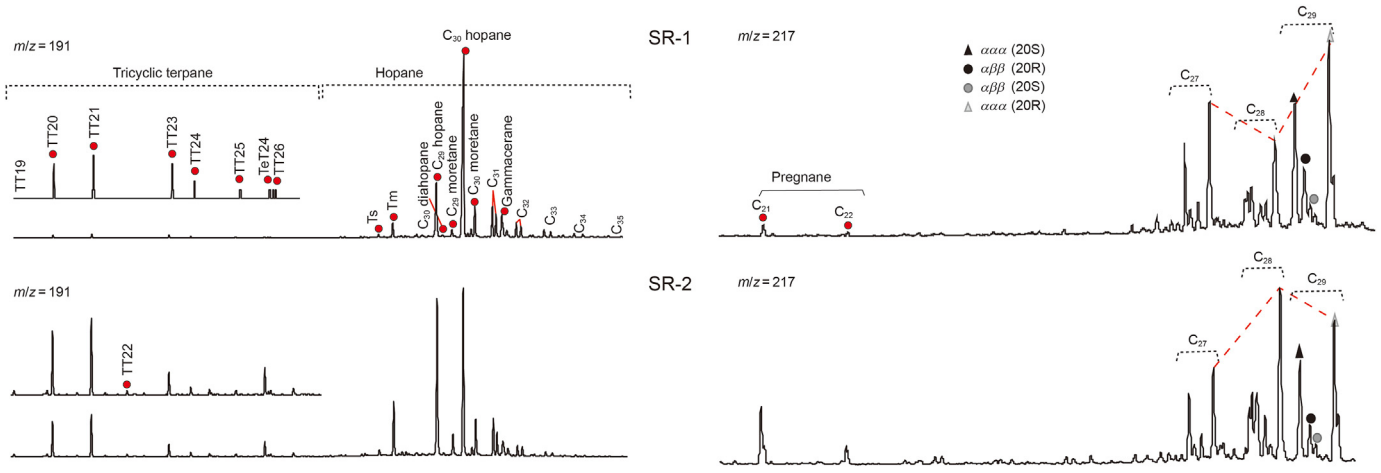

Fig. 5. Partial *m/z* 191 and 217 mass chromatograms showing the distribution of pentacyclic terpanes and steranes. TT: tricyclic terpane; TeT: tetracyclic terpane.

1993; Hunt, 1995). The Pr/Ph ratio represents the redox conditions during the precipitation of organic matter in the samples (Didyk et al., 1978; Mello et al., 1988). Furthermore, the Ph content is representative of the relative salinity of sedimentary water bodies (Connan and Cas Sou, 1980; Moldowan, 1985; Shanmugam, 1985; Peters and Moldowan, 1993). The higher the Ph content is, the greater is the salinity of the water column. In general, Pr and Ph are abundantly sourced from chlorophyll a of photosynthetic organisms (Powell and McKirdy, 1973). The relative contents of Pr and Ph can be characterized by the parameters Pr/nC_{17} and Ph/nC_{18}, respectively (Connan and Cas Sou, 1980; Shanmugam, 1985). The pristane/phytane (Pr/Ph) ratio values of shale samples vary mainly from 0.48 to 2.10 (Table 4). This indicates that shales were mainly deposited in a dysoxic environments. Fig. 6a shows the relationship between the Pr/nC_{17} and Ph/nC_{18} ratios of source rocks in the upper member of the Lucaogou Formation; these ratios were distributed over a wide range, showing the heterogeneity of organic matter composition of the source rocks in the upper member of the Lucaogou Formation. However, most of the data points of samples fall in the ranges of SR-1 and SR-2, which act as the two end-members in Fig. 6. It can also be found from Fig. 7a and b that as the content of telalginite increases, the ratio of Pr/nC_{17} and Ph/nC_{18} gradually increases. Therefore, Pr and Ph in the Lucaogou Formation are mainly derived from telalginite. Moreover, the higher content of Pr and Ph in the sample SR-1 indicates that telalginite is rich in chlorophyll a.

In general, β-carotane is observed in the TIC and $m/z = 125$ spectrogram (Fig. 4) and it is derived from β-carotene, which is the moiety of various pigments during the photosynthesis of organisms. Algae, photosynthetic bacteria, and higher plants are considered the biological sources of β-carotane (Hall and Douglas, 1981; Jiang and Flower, 1986). Although β-carotane is provided by phototrophs, it is less abundant in sedimentary rocks or oils because unsaturated carotenoids providing β-carotene are easily oxidized and destroyed (Peters et al., 2005). The content of β-carotane can be expressed by β-carotane/nC_{max} (Luo et al., 2018), which is in a large distribution range and approximates zero for most samples, such as the sample SR-2 which was dominated by lamalginite. Most of the samples contain a certain amount of β-carotane; however, the SR-1 samples dominated by telalginite showed a higher level of β-carotane. In addition, there is a positive correlation between β-carotane/nC_{max} and telalginite content (Fig. 7c). Therefore, the above mention indicates that the β-carotane is mainly sourced from telalginite in the study area, which is developed in a water column with higher salinity.

Numerous studies have shown that the short-chain *n*-alkanes ($< C_{20}$) are mostly found in algae and microorganisms (Cranwell, 1977). High-carbon-numbered *n*-alkanes are typical of terrestrial higher plants, and they mainly comprise plant wax (Eglinton and Hamilton, 1967; Bray and Evans, 1961). The terrigenous/aquatic ratio (TAR) index is calculated using the $(C_{27}+C_{29}+C_{31})/(C_{15}+C_{17}+C_{19})$ equation (Bourbonniere and Meyers, 1996). Fig. 6c shows that most data points of the samples are within the parameters range represented by lamalginite (SR-2) and telalginite (SR-1) and the input of organic matter to the sample dominated by telalginite increases in the direction that has a higher TAR index and a lower $C_{21}-/C_{22}+$. This is consistent with the positive correlation between the telalginite content and the TAR ratio parameter shown in Fig. 7d. The results showed that telalginite developed under high salinity conditions can also form *n*-alkanes with high carbon numbers. The *n*-alkanes in crude oil are mainly sourced from the lipids (Peters et al., 2005). Further, the long-chained lipids are more likely to degrade during the hydrocarbon generation by kerogen cracking than the short-chained lipids (Moldowan, 1985). The samples rich in telalginite represented high TAR index and low $C_{21}-/C_{22}+$ ratios, which suggests higher content of long-chain lipids in telalginite than that in lamalginite. It also indicates that telalginite has lower activation energy for hydrocarbon generation than lamalginite.

Tricyclic and tetracyclic terpanes have complex biological precursors and their origins have been controversial (Aquito Neto et al., 1983; Peters et al., 2005). In this study, the parameters of C_{20}TT/C_{23}TT, C_{21}TT/C_{23}TT, and C_{24}TeT/C_{26}TT ratios were used to express the relative content of different compounds. As the contribution of lamalginite increased, the contents of C_{20}TT, C_{21}TT, and C_{24}TeT in the selected samples demonstrated a significant increase as well (Fig. 8a and b; Fig. 9a, b and c). This indicates that lamalginite in the Lucaogou Formation is the source of C_{20}TT, C_{21}TT, and C_{24}TeT.

It was previously believed that C_{29} norhopane has a variety of sources; however, it is relatively developed in carbonate or

Table 5
Data of cumulative hydrocarbon generation rate and temperature of the samples in this study.

Temperature, °C	SR-1				SR-2			
	20, °C/min	30, °C/min	40, °C/min	50, °C/min	20, °C/min	30, °C/min	40, °C/min	50, °C/min
200	0	0	0	0	0	0	0	0
205	1.01	0.14	0.08	0.06	0.03	0.03	0.02	0.03
210	1.72	0.24	0.14	0.1	0.06	0.06	0.04	0.05
215	2.36	0.35	0.2	0.14	0.09	0.09	0.06	0.08
220	2.97	0.46	0.27	0.19	0.11	0.12	0.08	0.1
225	3.58	0.59	0.35	0.24	0.13	0.14	0.1	0.12
230	4.18	0.72	0.44	0.31	0.16	0.17	0.11	0.14
235	4.78	0.87	0.54	0.38	0.18	0.19	0.13	0.17
240	5.38	1.03	0.66	0.47	0.2	0.21	0.15	0.19
245	5.97	1.2	0.78	0.57	0.22	0.24	0.16	0.21
250	6.56	1.38	0.92	0.68	0.24	0.26	0.18	0.23
255	7.16	1.58	1.07	0.8	0.27	0.28	0.2	0.25
260	7.74	1.78	1.23	0.93	0.29	0.31	0.21	0.27
265	8.32	1.99	1.39	1.07	0.31	0.33	0.23	0.29
270	8.9	2.2	1.56	1.21	0.33	0.35	0.25	0.31
275	9.47	2.42	1.74	1.36	0.35	0.38	0.27	0.34
280	10.05	2.65	1.92	1.51	0.38	0.4	0.28	0.36
285	10.62	2.88	2.11	1.67	0.4	0.43	0.3	0.38
290	11.2	3.13	2.31	1.84	0.43	0.46	0.32	0.4
295	11.78	3.39	2.51	2.01	0.46	0.49	0.35	0.43
300	12.38	3.66	2.73	2.2	0.49	0.52	0.37	0.46
305	12.99	3.95	2.97	2.39	0.52	0.56	0.4	0.48
310	13.62	4.26	3.22	2.6	0.57	0.6	0.43	0.52
315	14.29	4.6	3.5	2.83	0.62	0.64	0.46	0.55
320	14.99	4.98	3.8	3.08	0.68	0.69	0.5	0.59
325	15.76	5.41	4.15	3.36	0.76	0.75	0.55	0.64
330	16.58	5.9	4.54	3.67	0.85	0.83	0.6	0.69
335	17.49	6.47	4.99	4.03	0.97	0.91	0.68	0.76
340	18.51	7.14	5.51	4.45	1.13	1.03	0.77	0.84
345	19.71	7.94	6.12	4.95	1.34	1.17	0.88	0.94
350	21.17	8.93	6.86	5.55	1.63	1.36	1.03	1.08
355	22.93	10.18	7.78	6.28	2.03	1.61	1.24	1.26
360	25.05	11.72	8.93	7.18	2.6	1.94	1.52	1.51
365	27.64	13.67	10.39	8.3	3.45	2.43	1.94	1.87
370	30.75	16.09	12.31	9.72	4.76	3.18	2.6	2.41
375	34.54	19.28	14.81	11.61	6.75	4.4	3.67	3.26
380	39.23	23.47	18.09	14.09	10.27	6.43	5.47	4.68
385	44.96	28.78	22.56	17.42	16.49	10	8.4	6.91
390	51.68	35.63	28.62	22.01	26.14	15.46	12.38	10.05
395	59.46	44.33	36.64	28.26	37.9	22.6	17.37	14.18
400	67.22	54.59	46.69	36.55	50.25	31.28	23.94	19.49
405	73.99	64.9	57.99	46.53	61.29	41.18	32.85	26.62
410	78.95	74.16	69.2	57.85	71.78	52.5	44.24	36.18
415	82.2	80.87	78.36	68.92	80.57	64	55.98	47.9
420	84.31	85.11	84.51	78.22	86.75	75.25	68.62	59.54
425	85.73	87.72	88.1	84.77	90.7	84	80.09	71.41
430	86.78	89.42	90.21	88.6	92.47	89.01	87.62	81.99
435	87.62	90.59	91.58	90.77	93.39	91.53	91.32	88.79
440	88.32	91.46	92.54	92.14	94.01	92.81	93.03	92.09
445	88.93	92.14	93.26	93.08	94.49	93.71	93.93	93.62
450	89.5	92.71	93.85	93.79	94.9	94.36	94.6	94.44
455	90.02	93.2	94.33	94.34	95.26	94.87	95.16	94.98
460	90.51	93.64	94.76	94.8	95.58	95.28	95.62	95.45
465	90.98	94.04	95.13	95.2	95.87	95.65	96.01	95.87
470	91.43	94.41	95.48	95.55	96.14	95.97	96.34	96.22
475	91.86	94.76	95.79	95.87	96.38	96.26	96.64	96.53
480	92.27	95.08	96.08	96.16	96.62	96.53	96.91	96.81
485	92.67	95.39	96.35	96.43	96.83	96.77	97.16	97.05
490	93.06	95.68	96.61	96.69	97.04	97	97.38	97.28
495	93.44	95.96	96.85	96.92	97.23	97.21	97.58	97.48
500	93.81	96.22	97.08	97.15	97.41	97.41	97.78	97.67
505	94.18	96.48	97.3	97.36	97.59	97.61	97.96	97.85
510	94.54	96.73	97.5	97.56	97.76	97.79	98.13	98.02
515	94.89	96.97	97.7	97.76	97.92	97.97	98.29	98.18
520	95.23	97.2	97.89	97.94	98.08	98.13	98.44	98.33
525	95.57	97.43	98.08	98.12	98.23	98.29	98.58	98.47
530	95.91	97.65	98.25	98.29	98.37	98.44	98.71	98.61
535	96.24	97.86	98.42	98.45	98.51	98.59	98.84	98.74
540	96.56	98.07	98.59	98.61	98.65	98.73	98.96	98.86
545	96.88	98.26	98.74	98.76	98.78	98.86	99.07	98.98
550	97.19	98.46	98.9	98.9	98.91	98.99	99.18	99.1
555	97.5	98.65	99.04	99.04	99.04	99.11	99.29	99.21

(*continued on next page*)

Table 5 (*continued*)

Temperature, °C	SR-1				SR-2			
	20, °C/min	30, °C/min	40, °C/min	50, °C/min	20, °C/min	30, °C/min	40, °C/min	50, °C/min
560	97.8	98.83	99.18	99.18	99.16	99.23	99.39	99.31
565	98.1	99	99.32	99.31	99.28	99.35	99.49	99.42
570	98.4	99.18	99.45	99.43	99.39	99.46	99.59	99.52
575	98.69	99.34	99.57	99.54	99.51	99.57	99.68	99.61
580	98.98	99.51	99.69	99.66	99.62	99.68	99.77	99.71
585	99.26	99.67	99.81	99.77	99.73	99.78	99.86	99.8
590	99.55	100	100	99.87	99.83	100	100	99.89
595	100	100	100	100	100	100	100	100
600	100	100	100	100	100	100	100	100

Table 6
The characteristics of transformation rate of hydrocarbon generation of the investigating samples.

Samples	Heating rate, °C/min	Temperature, °C			
		Hydrocarbon generation conversion: 10%	Hydrocarbon generation conversion: 50%	Hydrocarbon generation conversion: 90%	The temperature span (10%–90%)
SR-1	20	280	355	455	175
	30	355	400	435	80
	40	365	405	430	65
	50	375	410	425	50
SR-2	20	380	400	425	45
	30	385	410	430	45
	40	390	415	435	45
	50	390	415	435	45

Table 7
Hydrocarbon generation rate and activation energy data distribution data of the samples in this study.

Activation energies, kJ/mol	Hydrocarbon generation rate HC, %-SR-1	Hydrocarbon generation rate HC, %-SR-2
105–120	1	0
120–135	2	0
135–150	1	0
150–165	1	1
165–180	3	0
180–195	2	0
195–210	3	2
210–225	2	4
225–240	2	2
240–255	4	1
255–270	6	18
270–285	4	18
285–300	6	11
300–315	9	5
315–330	3	3
330–345	3	5
345–360	2	2
360–375	2	1
375–390	2	1
390–405	1	2
405–420	1	1
420–435	1	1
435–450	0	1
450–465	1	0
465–480	1	1
480–495	0	0
495–510	0	0
510–525	0	1
525–540	1	0
540–555	0	0
555–570	0	0
570–585	0	0
585–600	0	0

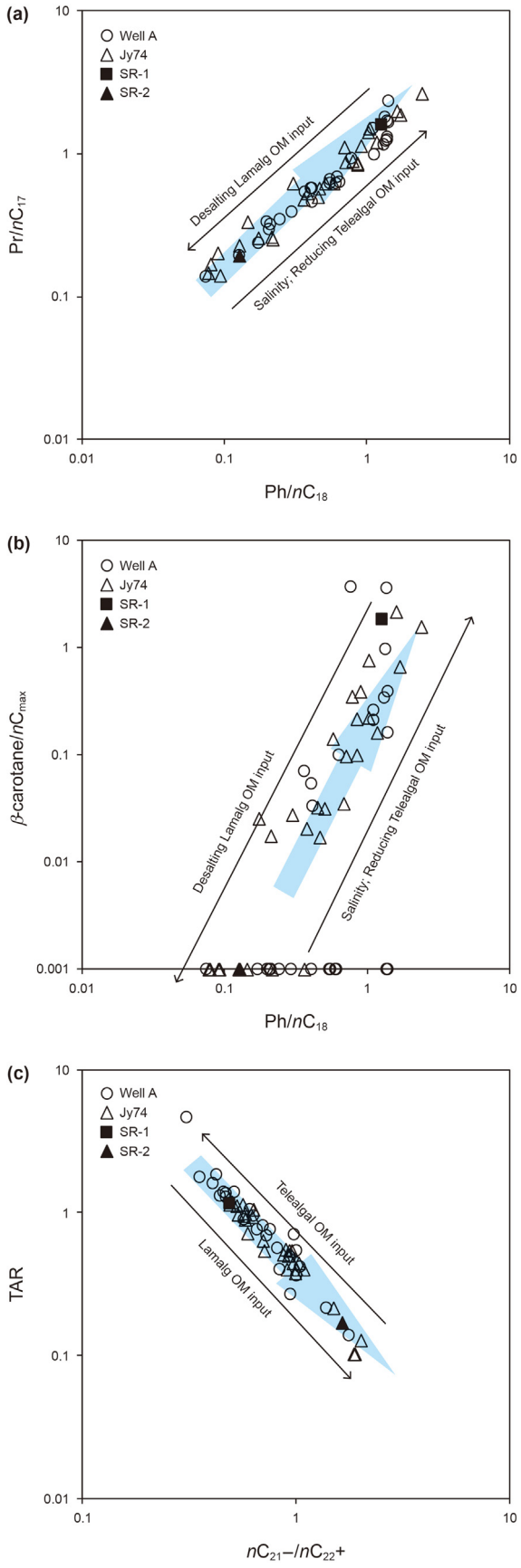

evaporite sedimentary environments (Zumberge, 1984; Connan et al., 1986; Clark and Philp, 1989; Ten Haven et al., 1988). Fig. 8c suggests that the $C_{29}\alpha\beta/C_{30}\alpha\beta$ hopane ratio values of most of the samples from the Lucaogou Formation fall between the two end members represented by Samples SR-1 and SR-2, and the $C_{29}\alpha\beta/C_{30}\alpha\beta$ hopane ratio values increase with the increase of lamginite content (Fig. 9d), indicating that lamalginite is the primary source of C_{29} norhopane in Lucaogou Formation.

The relative content of C_{27}–C_{28}–C_{29} regular steranes is often used to determine the biological origin of source rock samples (Huang and Meinschein, 1979; Volkman and Maxwell, 1986). Fig. 8d shows that sample SR-1, which is dominated by telalginite, falls in the zone of $C_{29} > C_{27} > C_{28}$ regular sterane and sample SR-2, which is dominated by lamalginite, falls in the $C_{28} > C_{29} > C_{27}$ region. Moreover, The C_{28}/C_{29} regular sterane ratio is positively correlated with the content of lamalginite, and negatively correlated with the content of telalginite (Fig. 9e and f). Therefore, the relationship between maceral content and biomarker compounds mentioned above indicates that lamalginite is the primary source of C_{28} regular steranes; however, C_{29} steranes is mainly soured from telalginite. Most data points of the samples in the study area fall in the zone of $C_{29} > C_{28} > C_{27}$ regular sterane, indicating that the hydrocarbon-generating parent material in most source rocks in the upper member of the Lucaogou Formation originates from of mixed lamalginite and telalginite in different proportions.

5.2. Thermal evolution and hydrocarbon generation characteristics

Based on the abovementioned research, the C_{28}/C_{29} regular sterane ratios were used to reflect the proportions of telalginite and lamalginite in hydrocarbon-generating parent materials for the Lucaogou Formation source rocks because they are seldom affected by thermal evolution. T_{max} is the temperature corresponding to the highest rate of hydrocarbon production from rock pyrolysis (Lu, 2008), which can indicate the level of thermal maturation as well as the presence of migrated hydrocarbons (Peters and Cassa, 1994). The T_{max} (445 °C) of sample SR-1 was lower than that of sample SR-2 (452 °C), but the buried depth and R_o of the two samples are not much different (Tables 1 and 2). Moreover, the pyrogram of the two samples displayed in Fig. 10a shows that sample SR-2 generated a large amount of hydrocarbons later compared with sample SR-1. In addition, Fig. 10b and c exhibit the Tmax frequency histograms of samples dominated by telalginite (C_{28}/C_{29} regular sterane < 0.75) and lamalginite (C_{28}/C_{29} regular sterane > 0.75), respectively. From Fig. 10b and c, it can be seen that the T_{max} distribution of the samples dominated by telalginite is significantly lower than that in the sample dominated by lamalginite. Therefore, the variation in the T_{max} value may not only be related to thermal evolution, but may also be directly related to the source of organic matter, and in this region, T_{max} cannot be used as an effective indicator of source rock maturity.

The abovementioned analytical results indicate that the organic matters in the source rocks of the Lucaogou Formation are heterogeneously sourced, resulting in differences in the maceral, which ultimately result in changes in the characteristics of hydrocarbon generation. The TOC and S_2 parameters in the source rocks can be used to evaluate the quality of the source rocks (Huang et al., 1984; Cheng, 1994; Gao et al., 2016). In Fig. 11, both the samples dominated by telalginite ($C_{28}/C_{29} < 0.75$) and those dominated by lamalginite ($C_{28}/C_{29} > 0.75$) exhibit good hydrocarbon-generating

Fig. 6. Cross plots of Pr/nC_{17} versus Ph/nC_{18} ratios (**a**), β-carotane/nC_{max} ratio versus Ph/nC_{18} ratio (**b**) and TAR ratio versus $nC_{21}-/nC_{22}+$ (**c**) of the Lucaogou Formation shale samples. TAR= $(nC_{27}+nC_{29}+nC_{31})/(nC_{15}+nC_{17}+nC_{19})$.

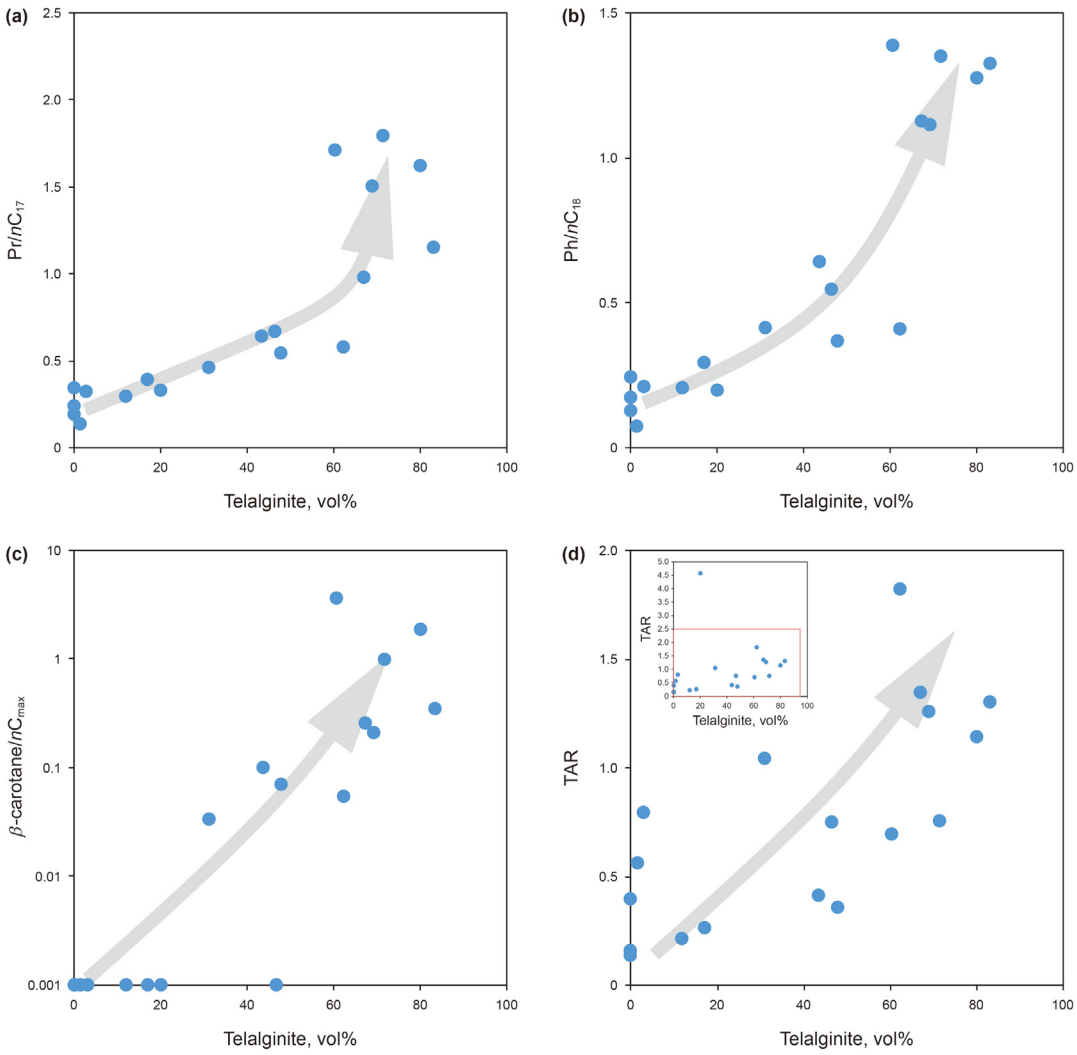

Fig. 7. Cross plots of telalginite versus Pr/nC$_{17}$ (**a**), Ph/nC$_{18}$ (**b**), β-carotane/nC$_{max}$ (**c**) and TAR (**d**) ratio of the Lucaogou Formation shale samples in Well A.

potential. Most of the samples are distributed in the range of good-excellent source rocks dominated by oil-prone organic matter (Fig. 11).

Among various organic geochemical analytical methods, Rock–Eval pyrolysis S_1 generally represents the amount of residual hydrocarbons that have been generated in the source rock that can approximately represent the amount of hydrocarbon generation in source rocks without hydrocarbon expulsion. The content of EOM obtained by extraction can directly represent the hydrocarbons detained in the source rocks (Peters et al., 2005; Gao et al., 2016). Based on the abovementioned principles, Fig. 12a and c show that the S_1 and EOM% parameters in most samples have a negative correlation with the C$_{28}$/C$_{29}$ regular sterane for the study samples, respectively; however, some sample points deviate from the correlation trend. This is because the S_1 and EOM parameters are also related to the abundance of organic matter in rock samples; the higher the abundance of organic matter is, the higher would the corresponding S_1 and EOM values be. Fig. 12b and d shows the relationship between the residual hydrocarbon generation per organic matter (HCI: S_1/TOC×100; EOM/TOC) and the C$_{28}$/C$_{29}$ regular steranes. Fig. 12 shows that most samples fall within the normal trend, indicating that at the current maturity, the hydrocarbon-generation conversion rate of telalginite is higher than that of lamalginite.

The sterane isomerization parameters of ααα20S/(20S+20R) C$_{29}$ sterane ratio and ββ/(αα+ββ) of C$_{29}$ sterane ratio are considered to be effective maturity parameters (the equilibrium points fall in the ranges of 0.52–0.55 and 0.67–0.71 (Seifert and Moldowan, 1986), respectively). Previous studies have shown that the organic matter deposited in high salinity has the characteristics of early hydrocarbon generation, and the related isomerization parameters of steranes and terpenes will reach the end of equilibrium at the lower thermal evolution stage (ten Haven et al., 1985, 1986; Zumberge, 1984; Köster et al., 1997). The ααα20S/(20S+20R) C$_{29}$ and ββ/(αα+ββ) of C$_{29}$ sterane ratios of most samples decrease as the C$_{28}$/C$_{29}$ regular sterane increases (Fig. 13a and b), which suggests that lamalginite enters the evolution stage of hydrocarbon generation later than telalginite. In Fig. 14, the relationship between biomarker parameters of the sample and the depth is displayed. When the vitrinite reflectance was greater than 0.77% (the measured points of

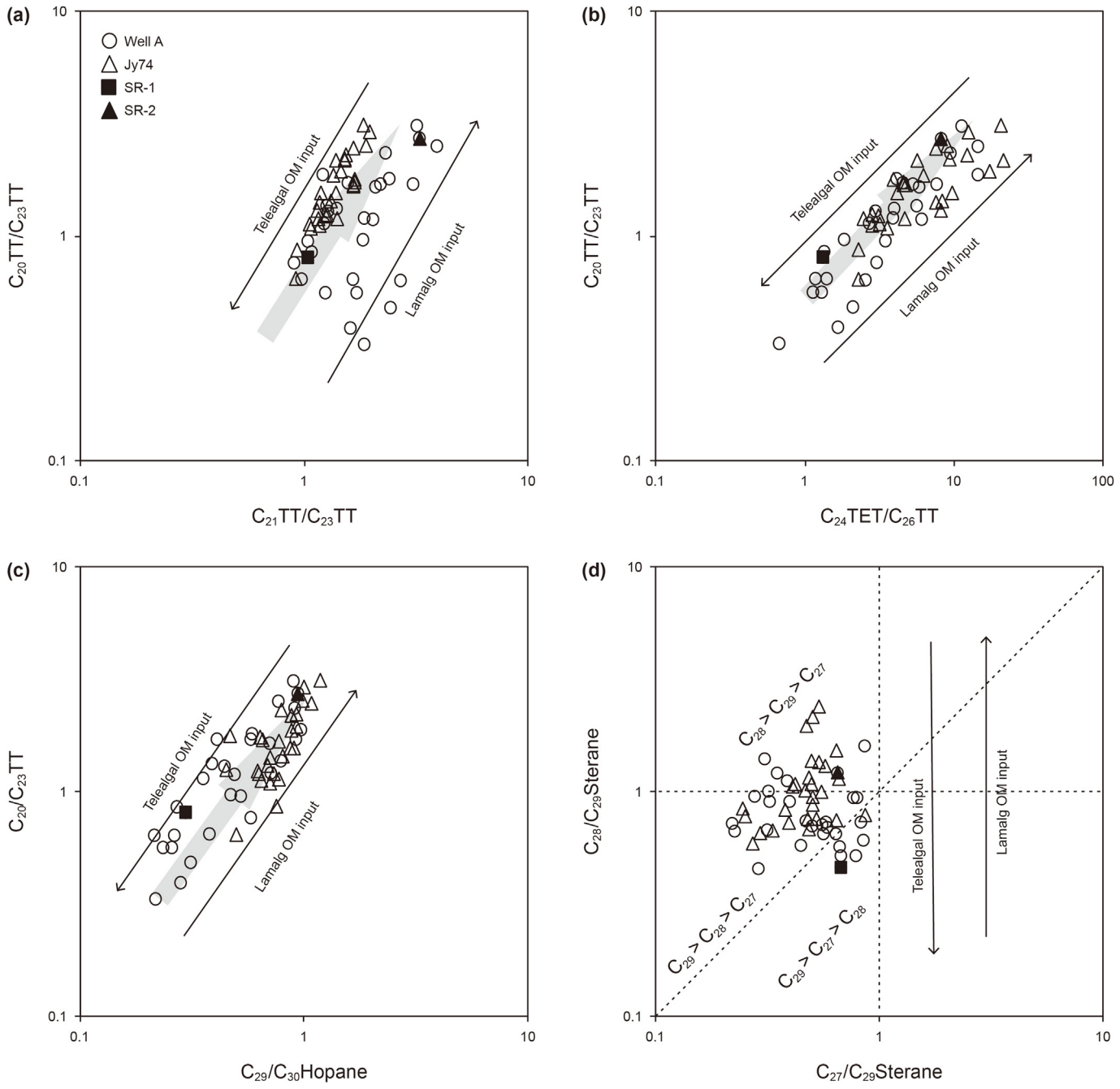

Fig. 8. Cross plots of $C_{20}TT/C_{23}TT$ ratios versus $C_{21}TT/C_{23}TT$ ratios (**a**), $C_{24}TET/C_{26}TT$ ratio (**b**), C_{29}/C_{30} Hopane ratio (**c**) and C_{27}/C_{29} Sterane ratios versus C_{28}/C_{29} Sterane ratios (**d**) of the Lucaogou Formation shale samples.

samples, Table 1), the ααα20S/(20S+20R) C_{29} sterane ratio of the sample in Well A reached the equilibrium endpoint (Fig. 14c). However, the ββ/(αα+ββ) of C_{29} sterane ratios began to increase significantly (Fig. 14b). This is because the ββ/(αα+ββ) of C_{29} sterane ratios reached equilibrium at a slower rate than ααα20S/(20S+20R) C_{29} sterane ratio (Seifert and Moldowan, 1986). By comparing Figs. 13 and 14, it can be concluded that the higher ββ/(αα + ββ) of the C_{29} sterane ratios sample in Fig. 13b are attributed to the deeper burial depth and the higher telalginite input. The ααα20S/(20S+20R) C_{29} sterane ratios of samples in Well A are the result of reaching the end of equilibrium (Figs. 13b and 14c).

Various parameters from rock pyrolysis and biomarker analysis indicate that the source-rock samples of the upper member of the Lucaogou Formation are currently in the low-mature to mature stage. Moreover, telalginite has a higher hydrocarbon generation conversion rate than lamalginite in the early thermal evolution stage.

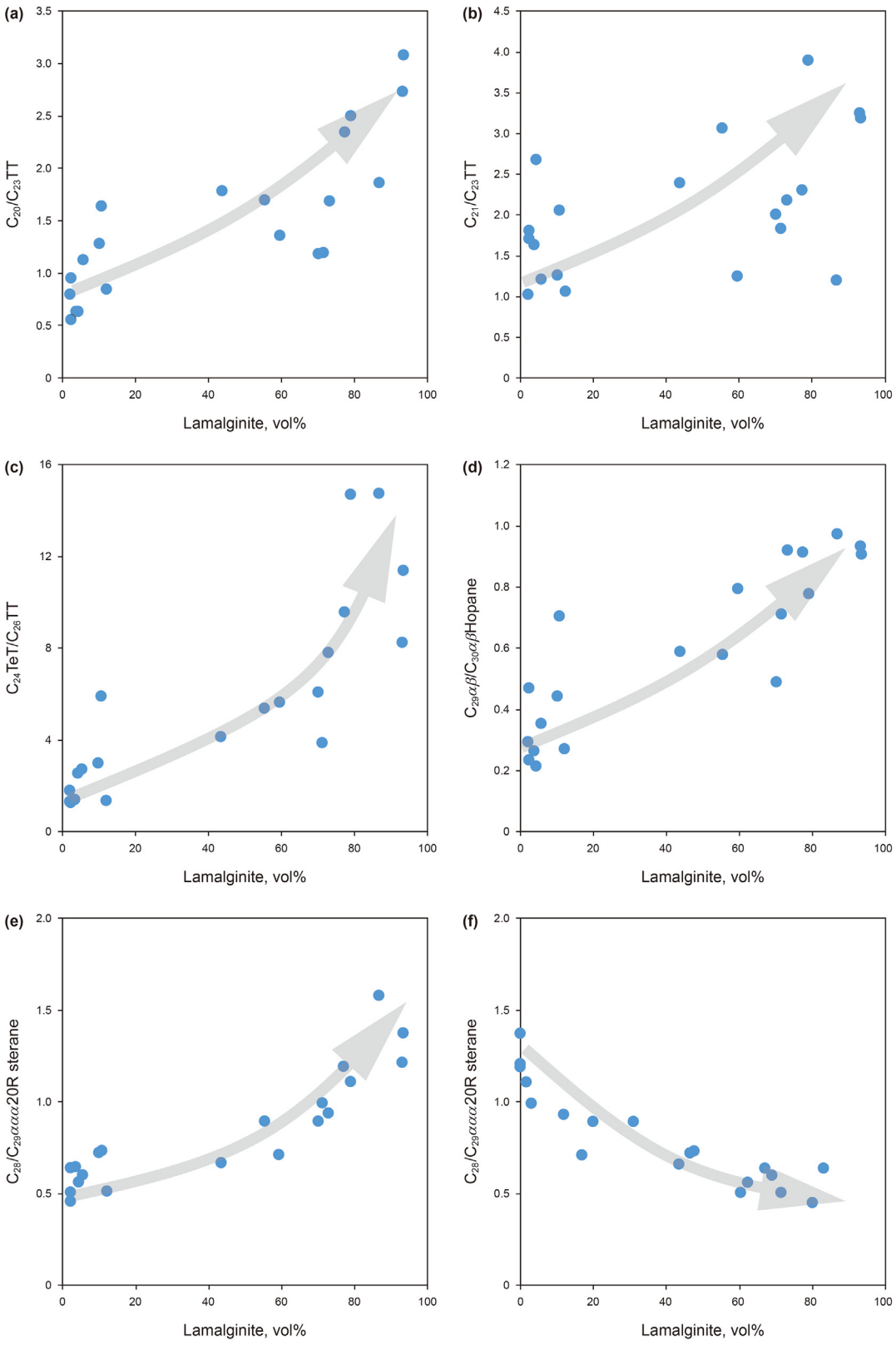

Fig. 9. Cross plots of lamalginite versus $C_{20}TT/C_{23}TT$ (**a**), $C_{21}TT/C_{23}TT$ (**b**), $C_{24}TET/C_{26}TT$ (**c**), C_{29}/C_{30} hopane (**d**) and C_{28}/C_{29} regular sterane (**e**) ratios and telalginite versus C_{28}/C_{29} regular sterane (**f**) ratios of the Lucaogou Formation shale samples in Well A.

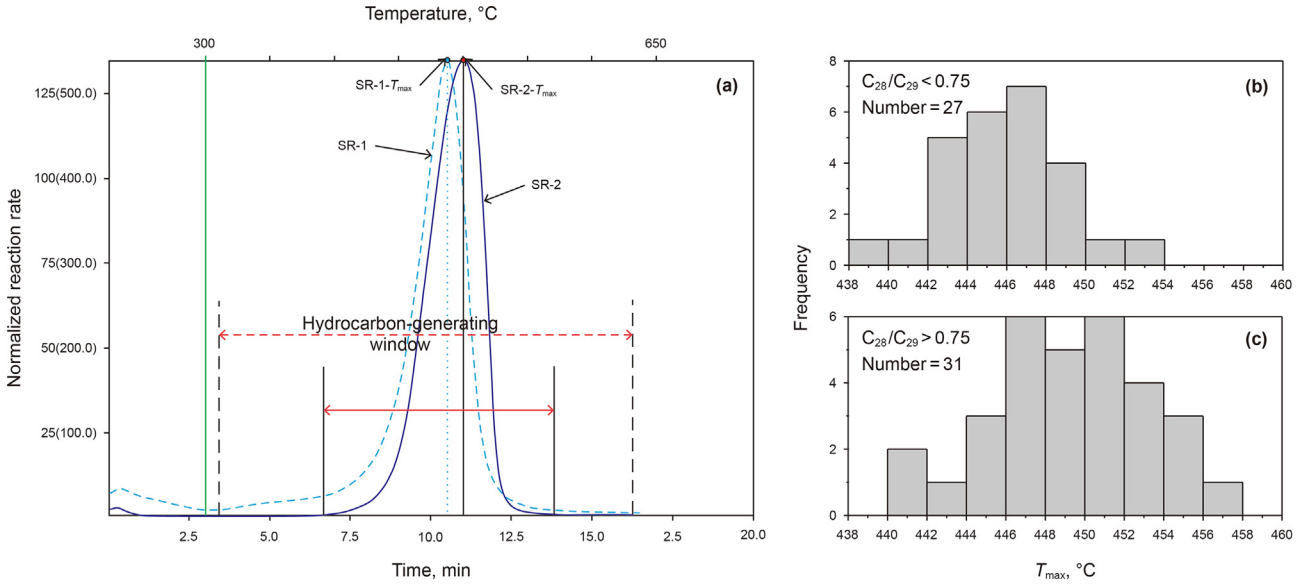

Fig. 10. Pyrolysis spectra of SR-1 and SR-2 samples (**a**); Histogram of T_{max} frequency distribution for $C_{28}/C_{29} < 0.75$ (**b**) and $C_{28}/C_{29} > 0.75$ (**c**). 25(100): The normalized reaction rate of SR-1 (The normalized reaction rate of SR-2). C_{28}/C_{29}: C_{28}/C_{29} regular sterane.

5.3. Activation energies of telalginite and lamalginite

The hydrocarbon generation conversion rate curves of the studied samples exhibit evidently distinct characteristics (Fig. 15a and c). The hydrocarbon generation characteristics of the samples were studied by considering the conversion rates of 10% and 90% as the lower limit and equilibrium point of the hydrocarbon generation of effective source rocks, respectively. A conversion rate of 50% is regarded as the conversion central axis. Table 6 shows that the temperatures at which SR-1 starts to generate hydrocarbons (20 °C/min: 280 °C, 30 °C/min: 335 °C, 40 °C/min: 365 °C, 50 °C/min: 375 °C) are lower than those of SR-2 (20 °C/min: 380 °C, 30 °C/min: 385 °C, 40 °C/min: 390 °C, 50 °C/min: 390 °C) (Table 6). The temperatures at which the SR-1 stops generating hydrocarbons (20 °C/min: 455 °C, 30 °C/min: 435 °C, 40 °C/min: 430 °C, 50 °C/min: 425 °C) are slightly higher than those of sample SR-2 (20 °C/min: 425 °C, 30 °C/min: 430 °C, 40 °C/min: 435 °C, 50 °C/min: 435 °C) (Table 6). The effective hydrocarbon-generating temperatures of telalginite (20 °C/min: 175 °C, 30 °C/min: 80 °C, 40 °C/min: 65 °C, 50 °C/min: 50 °C) were wider than those of lamalginite (20 °C/min: 45 °C, 30 °C/min: 45 °C, 40 °C/min: 45 °C, 50 °C/min: 45 °C) (Table 6). The activation energy distribution of telalginite was relatively wide, within the range of 120–390 kJ/mol, with an average activation energy of 259 kJ/mol (Fig. 15b) (Table 7). Conversely, the activation energy distribution of lamalginite is relatively concentrated, within the range of 255–315 kJ/mol, with an average activation energy of 245 kJ/mol (Fig. 15d) (Table 7). This indicates that the hydrocarbon generation of telalginite is characterized by lower initial hydrocarbon-generation activation energy, wide activation energy distribution, and slow reaction rate, whereas that of lamalginite is characterized by a higher initial hydrocarbon-generation activation energy, a narrow activation energy distribution, and high reaction rate (Fig. 16).

The hydrocarbon generation characteristics of telalginite and lamalginite have been studied in different basins globally. For example, the oil shale of the Green River Formation in the Green River Basin is rich in a large number of lamalginites (Katz, 1995) and

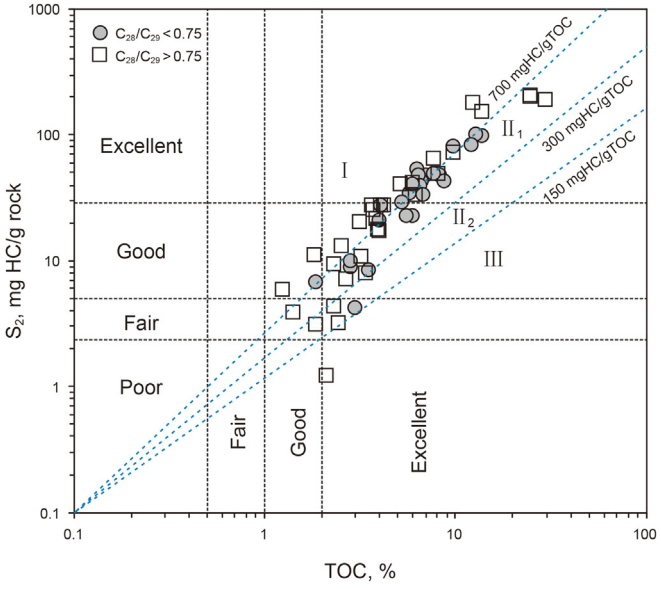

Fig. 11. Evaluation of the Lucaogou Formation source rock quality by intersection diagram of TOC and Rock-Eval S_2.

the activation energy distributions of the whole rock and kerogen of the shale in the Green River Formation are extremely narrow (Behar et al., 1997; Dieckmann, 2005) (Table 8). This indicates that lamalginite generally exhibits concentrated hydrocarbon generation. The source rocks of the Monterey Formation in the California Basin contain a large amount of telalginite (Rahman et al., 2017), which has a wide distribution of activation energy; moreover, the activation energy here at the beginning of hydrocarbon generation is relatively lower than that in source rocks of Green River Formation (Behar et al., 1997; Romero-Sarmiento et al., 2016) (Table 8). Generally, for most source rocks, the vitrinite reflectance at the beginning of oil generation is ~0.6% (Dow, 1977; Peters, 1986).

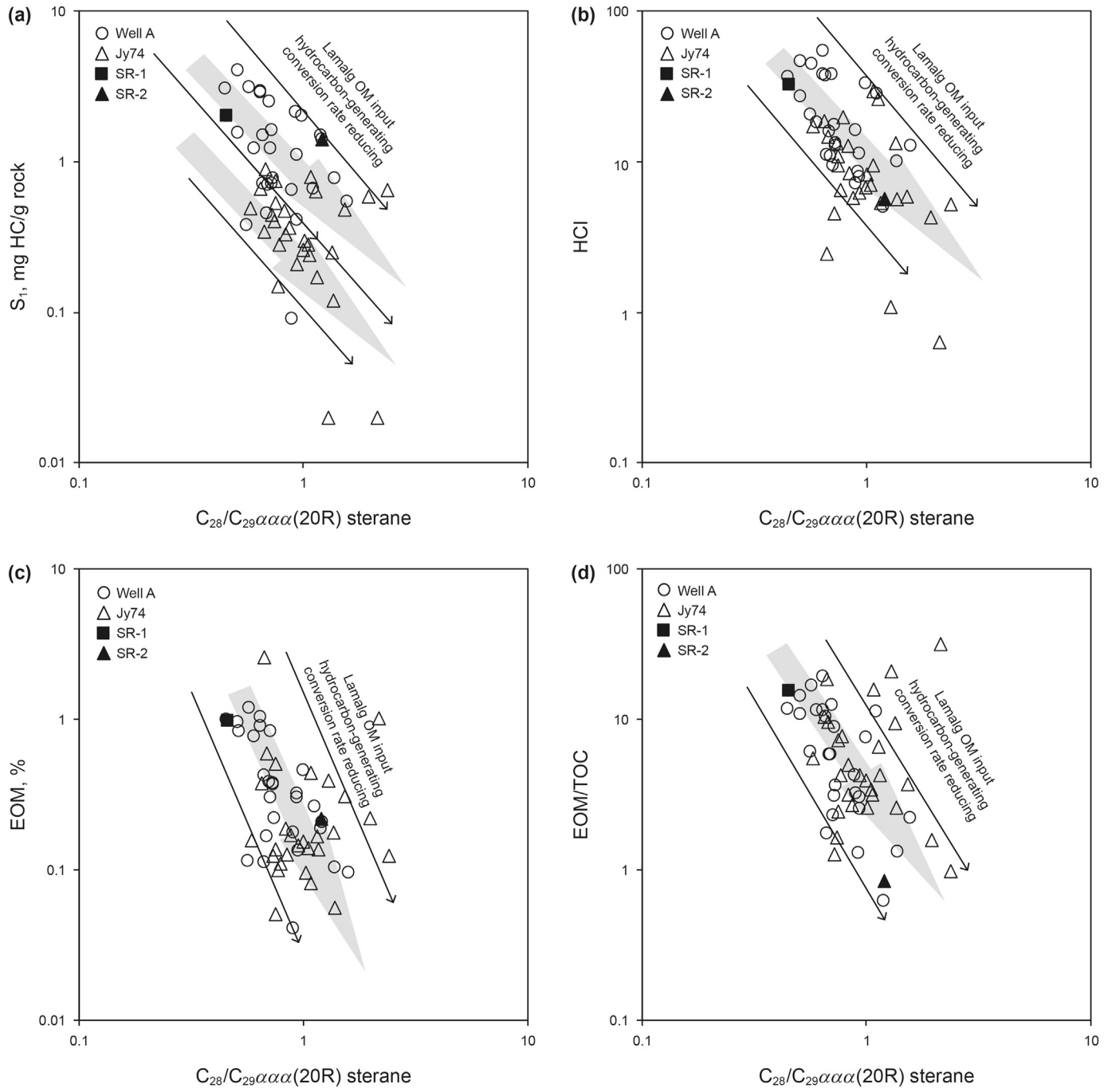

Fig. 12. Cross plots of C_{28}/C_{29} ααα (20R) sterane ratios versus S_1 values (**a**), HCI ratio (**b**), EOM values (**c**) and EOM/TOC ratios (**d**) of the Lucaogou Formation shale samples.

However, when the source rocks of the Monterey Formation has an $R_o = 0.3\%$, it is evident that a large amount of EOM has been produced (Isaacs and Rullkotter, 2000); Furthermore, for the source rocks of Green River Formation, the amount of oil produced when the R_o value is close to 0.7% reaches this level (Tissot et al., 1978). The difference in hydrocarbon generation between lamalginite and telalginite should be similar in a series of basins. Essentially, the hydrocarbon generation of organic matter depends on its chemical structure and material composition (Rullkotter et al., 1987; Schenk et al., 1997; Di Primio et al., 2000). Abarghani et al. (2019) studied the use of AFM–IR spectroscopy (nanoIR) to show that telalginite has a strong chemical heterogeneity. Fig. 2 shows that the fluorescence characteristics of telalginite and lamalginite are clearly different. The fluorescence of lamalginite represents homogeneity whereas that observed in the middle of telalginite and around it exhibits evident differences (Fig. 2). This also reflects that the

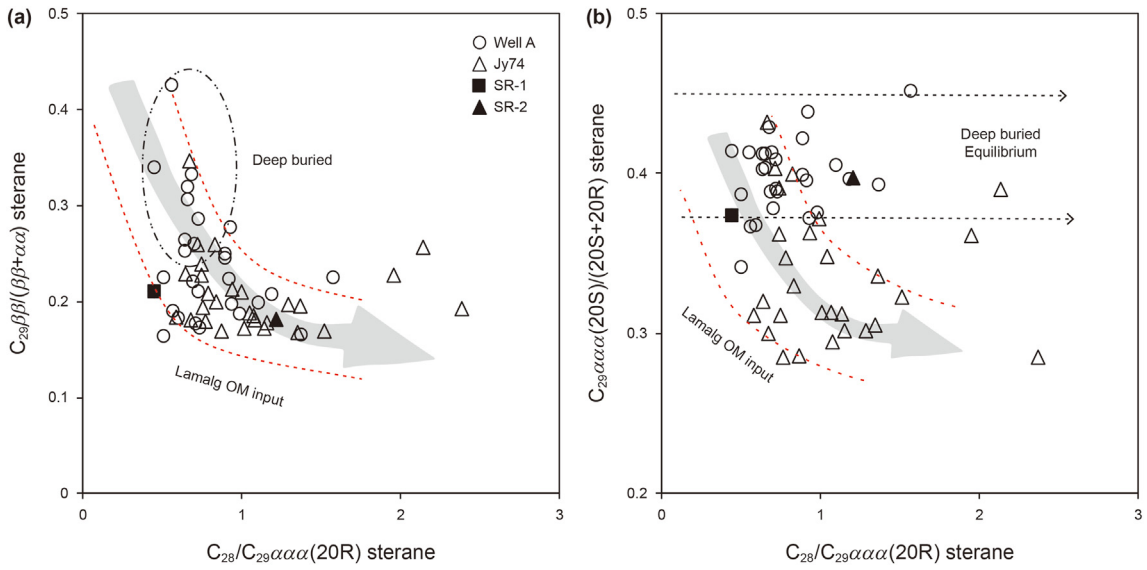

Fig. 13. Cross plots of C_{28}/C_{29} ααα (20R) sterane ratios versus C_{29} ββ/(αα+ββ) sterane ratios (**a**) and C_{29} ααα20S/(20S+20R) sterane ratios (**b**) of the Lucaogou Formation shale samples.

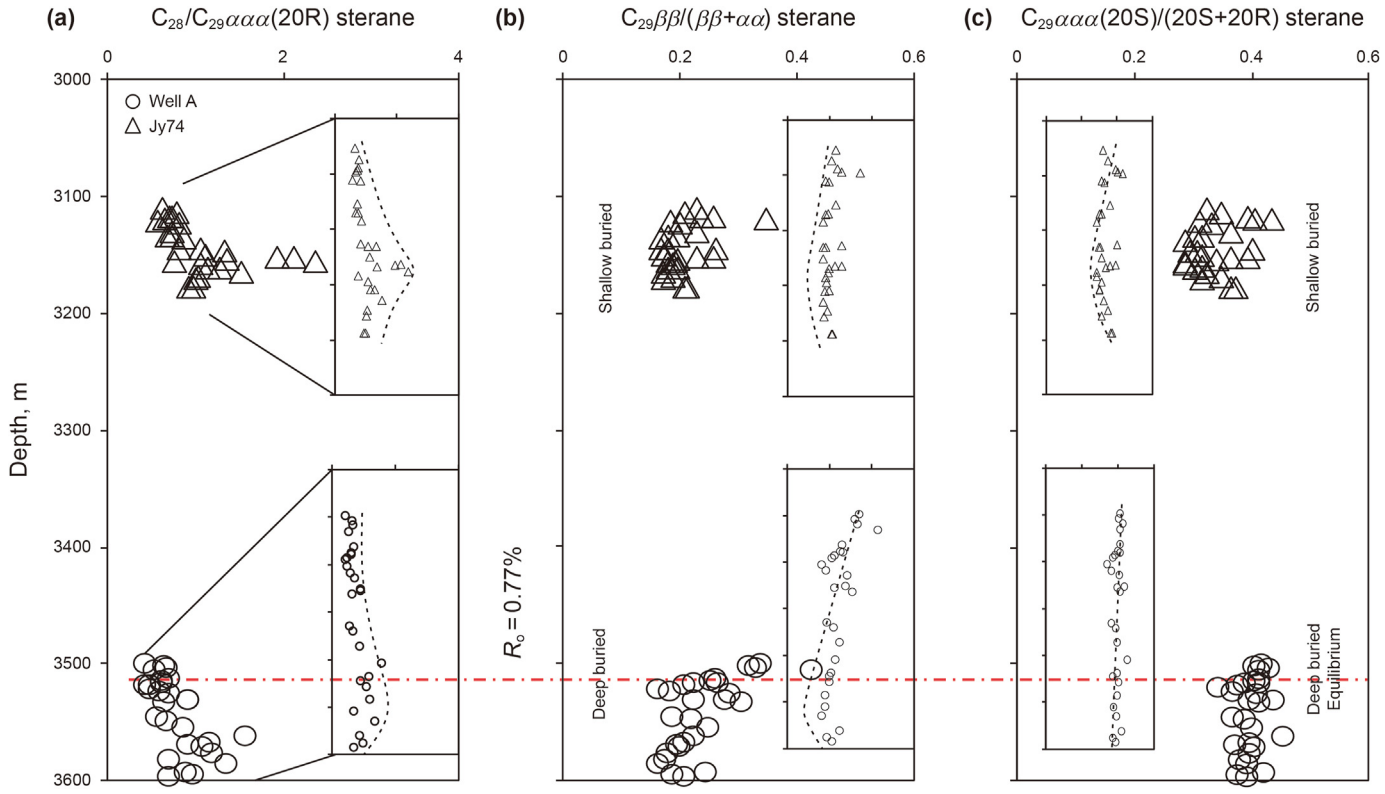

Fig. 14. Identification of organic inputs and maturity from steranes in the Lucaogou Formation mudstones of the Well A and JY74 (**a**) C_{28}/C_{29} ααα20R sterane versus depth (m). (**b**) C_{29} steranes αββ/(αββ+ααα) versus depth (m). (**c**) C_{29} steranes 20S/(20S+20R) versus depth (m).

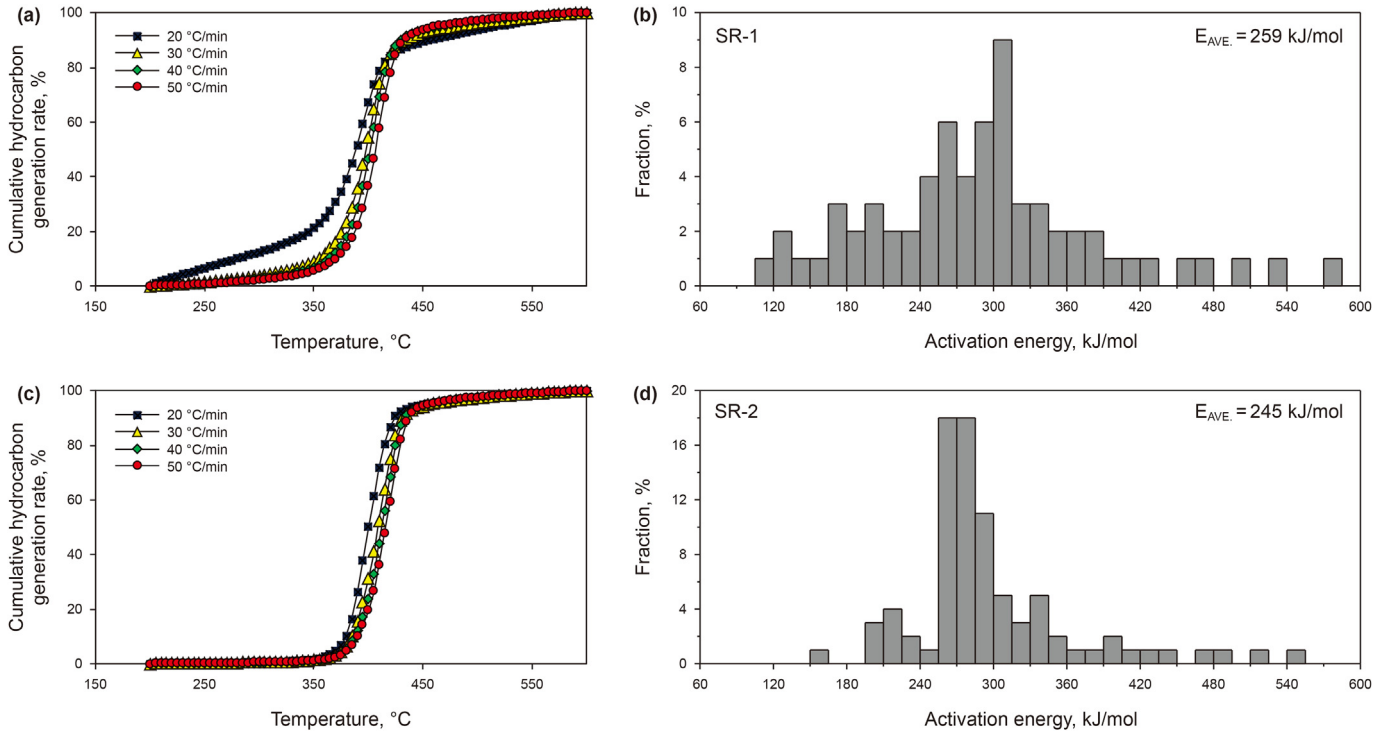

Fig. 15. Cumulative hydrocarbon generation rate (%) with increasing temperature during pyrolysis of the SR-1 (**a**) and SR-2 (**c**) samples from the Lucaogou Formation shale; Activation energy (Ea) distribution and frequency factor of SR-1 (**b**) and SR-2 (**d**) samples from the Lucaogou Formation shale.

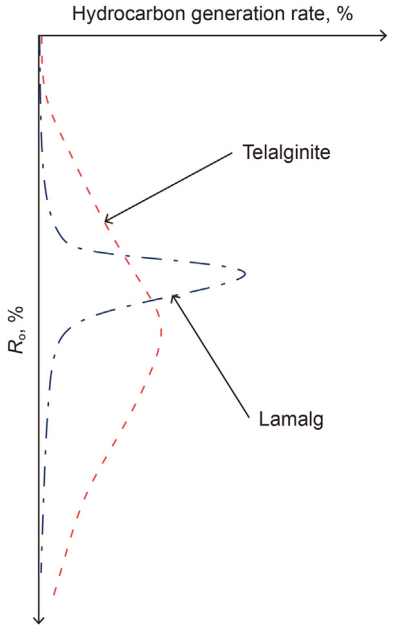

Fig. 16. Hydrocarbon generation patterns of telalginite and lamalginite of Lucaogou Formation in Jimusaer Sag.

chemical composition of lamalginite is simple, whereas a significant chemical heterogeneity is observed in the case of telalginite. Therefore, the activation energy of telalginite during degradation and hydrocarbon generation is wide and that of lamalginite is narrow.

6. Conclusions

Samples collected from the Lucaogou Formation containing typical hydrocarbon-generating parent materials were used to compare organic geochemical characteristics, hydrocarbon-generating characteristics, and hydrocarbon-generating kinetic characteristics.

The hydrocarbons formed by telalginite in the Lucaogou Formation have a high content of β-carotane, Pr, Ph, and relatively high content of C_{29} regular steranes. Lamalginite has high content C_{20}TT, C_{21}TT, C_{24} TeT, C_{29} norhopane, and C_{28} regular steranes. At present, the upper member of the Lucaogou Formation is in the low-mature to mature stage. Telalginite in the source rock of the Lucaogou Formation has a higher hydrocarbon conversion rate than that of lamalginite. The concentrated activation energy distribution of lamalginite shows that lamalginite has the characteristics of concentrated hydrocarbon generation, and telalginite has a wide distribution of activation energy, the characteristics of early oil generation, and a wide oil generation window.

Table 8
A synopsis of some published bulk kinetic experiments on shale.

Source rock	Sample type	Heating rates, K/min	Activation energy (Ea), kcal/mol	Frequency factor (1/S)	Pyrolysis method	Reference
Green River	Rock	0.1, 0.7, 5	Narrow (51–58) peak 56	1.11E+15	Open system	Dieckmann (2005)
	Kerogen	0.1, 0.7, 5	Very narrow (52–54) peak 54	7.40E+13	Open system	Behar et al. (1997)
Monterey	Rock	0.7, 2, 5,	wide(44–70) peak 53	5.89E+13	Open system	Rahman et al. (2017)
	Kerogen	2, 5, 10, 15	Wide (44–60) peak 48, 50	2.50E+13	Open system	Behar et al. (1997)

On a whole, this technology fully demonstrates the biomarker characteristics of the main macerals in the source rocks of the Lucaogou Formation, which is significant in providing some guidance for the biological sources of source rocks in other similar basins. The differences in hydrocarbon generation kinetics of different macerals lay a theoretical foundation for the shale oil enrichment mechanism and shale oil resource calculation in the Lucaogou Formation.

Acknowledgements

We would like to thank Xinjiang Oilfield Company for allowing the publication of the manuscript, and in particular, they have provided part of the geochemistry data of shales and stratigraphic framework for us.

References

Abarghani, A., Gentzis, T., Shokouhimehr, M., et al., 2019. Chemical heterogeneity of organic matter at nanoscale by AFM-based IR spectroscopy. Fuel 261, 116454. https://doi.org/10.1016/j.fuel.2019.116454.

Aquito Neto, F.R., Trendel, J.M., Restlé, A., et al., 1983. Occurrence and Formation of Tricyclic Terpanes in Sediments and Petroleums. Advances in Organic geochemistry. John Wiley & Sons, New York, pp. 659–676.

Bai, H., Pang, X.Q., Kuang, L.C., et al., 2017. Hydrocarbon expulsion potential of source rocks and its influence on the distribution of lacustrine tight oil reservoir, middle Permian Lucaogou Formation, Jimsar Sag , Junggar Basin , Northwest China. J. Petrol. Sci. Eng. 149, 740–755. https://doi.org/10.1016/j.petrol.2016.09.053.

Behar, F., Kressman, S., Rudkiewicz, J.L., et al., 1992. Experimental simulation in a confined system and kinetic modeling of kerogen and oil cracking. Org. Geochem. 19 (1), 173–189. https://doi.org/10.1016/0146-6380(92)90035-V.

Behar, F., Vandenbroucke, M., Tang, Y., et al., 1997. Thermal cracking of kerogen in open and closed systems: determination of kinetic parameters and stoichiometric coefficients for oil and gas generation. Org. Geochem. 26 (5–6), 321–339. https://doi.org/10.1016/S0146-6380(97)00014-4.

Bourbonniere, R.A., Meyers, P.A., 1996. Anthropogenic influences on hydrocarbon contents of sediments deposited in eastern Lake Ontario since 1800. Environ. Geol. 28 (1), 22–28. https://doi.org/10.1007/s002540050074.

Bray, E.E., Evans, E.D., 1961. Distribution of n-paraffins as a clue to recognition of source beds. Geochem. Cosmochim. Acta 22 (1), 2–15. https://doi.org/10.1016/0016-7037(61)90069-2.

Burnham, A.K., Sweeney, J.J., 1989. A chemical kinetic model of vitrinite maturation and reflectance. Geochem. Cosmochim. Acta 53 (10), 2649–2657. https://doi.org/10.1016/0016-7037(89)90136-1.

Cao, Z., Liu, G.D., Kong, Y.H., et al., 2016. Lacustrine tight oil accumulation characteristics: permian Lucaogou Formation in jimusaer sag, Junggar Basin. Int. J. Coal Geol. 153, 37–51. https://doi.org/10.1016/j.coal.2015.11.004.

Cao, Z., Liu, G.D., Xiang, B.L., et al., 2017. Geochemical characteristics of crude oil from a tight oil reservoir in the Lucaogou Formation, Jimusar sag, Junggar Basin. AAPG Bull. 101, 39–72. https://doi.org/10.1306/05241614182.

Cheng, K.M., 1994. Oil and Gas Generation of Tuha Basin. Petroleum Industry Press, Beijing (in Chinese).

Clark, J.P., Philp, R.P., 1989. Geochemical characterization of evaporate and carbonate depositional environments and correlation of associated crude oils in the Black Creek Basin, Alberta. Canadian Petrol. Geol. Bulletin 37 (4), 401–416. https://doi.org/10.1306/01111311128.

Connan, J., Bouroullec, J., Dessort, D., et al., 1986. The microbial input in a carbonate–anhydrite facies of a sabka paleoenvironment from Guatemala: a molecular approach. Org. Geochem. 10 (1–3), 29–50. https://doi.org/10.1016/0146-6380(86)90007-0.

Connan, L., Cas Sou, A.M., 1980. Properties of gases and petroleum liquids derived from terrestrial kerogen at various maturation levels. Geochimica Cosmchimica Acta 44, 1–23. https://doi.org/10.1016/0016-7037(80)90173-8.

Cranwell, P.A., 1977. Organic geochemistry of cam Loch (Sutherland) sediments. Chem. Geol. 20, 205–221. https://doi.org/10.1016/0009-2541(77)90044-4.

Di Primio, R., Horsfield, B., Guzman-Vega, M.A., 2000. Determining the temperature of petroleum formation from the kinetic properties of petroleum asphaltenes. Nature 406, 173–176. https://doi.org/10.1038/35018046.

Didyk, B., Simoneit, B., Brassell, S., et al., 1978. Organic geochemical indicators of palaeoenvironmental conditions of sedimentation. Nature 272, 216–222. https://doi.org/10.1038/272216a0.

Dieckmann, V., 2005. Modelling petroleum formation from heterogeneous source rocks: the influence of frequency factors on activation energy distribution and geological prediction. Mar. Petrol. Geol. 22, 375–390. https://doi.org/10.1016/j.marpetgeo.2004.11.002.

Dieckmann, V., Ondrak, R., Cramer, B., Horsfield, B., et al., 2006. Deep basin gas: new insights from kinetic modelling and isotopic fractionation in deep-formed gas precursors. Mar. Petrol. Geol. 23 (2), 183–199. https://doi.org/10.1016/j.marpetgeo.2005.08.002.

Domine, F., Dessort, D., Brevart, O., 1998. Toward a new method of geochemical kinetic modeling: implications for the stability of crude oils. Org. Geochem. 28 (9–10), 579–612. https://doi.org/10.1016/S0146-6380(98)00030-8.

Dow, W.G., 1977. Petroleum source beds on continental slopes and rises. AAPG Bull. 62 (9), 1584–1606. https://doi.org/10.1306/C1EA5256-16C9-11D7-8645000102C1865D.

Eglinton, G., Hamilton, R.J., 1967. Leaf epicuticular waxes. Science 156, 1322–1335. https://doi.org/10.1126/science.156.3780.1322.

Erdmann, M., Horsfield, B., 2006. Enhanced late gas generation potential of petroleum source rocks via recombination reactions: evidence from the Norwegian North Sea[J]. Geochem. Cosmochim. Acta 70, 3943–3956. https://doi.org/10.1016/j.gca.2006.04.003.

Fang, S., Xu, H., Song, Y., et al., 2005. Characteristics and evolution of the composite petroleum system in Jimsar depression, eastern Junggar Basin. Acta Geosci. Sin. 26 (3), 259–264 (in Chinese with English Abstract).

Fu, J.M., Shi, J.Y., 1975. Theory and practice about petroleum evolvement (I) :Theory and stages of petroleum evolvement. Geochi mica 4 (2), 87–110.

Gao, G., Zhang, W., Xiang, B.L., et al., 2016. Geochemistry characteristics and hydrocarbon–generating potential of lacustrine source rock in Lucaogou Formation of the Jimusaer Sag, Junggar Basin. J. Petrol. Sci. Eng. 145, 168–182. https://doi.org/10.1016/j.petrol.2016.03.023.

Hackley, P.C., Fishman, N., Wu, T., et al., 2016. Organic petrology and geochemistry of mudrocks from the lacustrine Lucaogou Formation, Santanghu Basin, northwest China: application to lake basin evolution. Int. J. Coal Geol. 168, 20–34. https://doi.org/10.1016/j.coal.2016.05.011.

Hall, P.B., Douglas, A.G., 1981. The distribution of cyclic alkanes in two lacstrine deposits. In: Hjoray, M., Albrecht, C., Cornford, C., et al. (Eds.), Advances in Organic Geochemistry. John Wiley & Sons, Chichester, UK, pp. 576–587.

Huang, D.F., Li, J.C., Gu, X.Z., 1984. Evolution and Hydrocarbon-Generating Mechanism of Terrigenous Organic Matter. Petroleum Industry Press, Beijing.

Huang, W.Y., Meinschein, W.G., 1979. Sterols as ecological indicators. Geochem. Cosmochim. Acta 43, 739–745. https://doi.org/10.1016/0016-7037(79)90257-6.

Hunt, J.M., 1995. Petroleum Geochemistry and Geology. W.H. Freeman and Company, New York.

Hutton, A.C., 1982. Organic Petrology of Oil Shales. PhD Thesis. University of Wollongong., p. 519

Hutton, A.C., 1987. Petrolographic classification of oil shales. Int. J. Coal Geol. 8, 203–231. https://doi.org/10.1016/0166-5162(87)90032-2.

ICCP, 2001. The new intertinite classification (ICCP system 1994). Fuel 80, 459–471.

ICCP, 1998. The new vitrinite classification (ICCP system 1994). Fuel 77, 349–358.

Isaacs, C.M., Rullkotter, J., 2000. The Monterey Formation: from Rocks to Molecules. Columbia University Press, New York.

Jiang, Z.S., Flower, M.G., 1986. Carotenoid derved alkanes in oil from Northwestern China. Org. Geochem. 10 (4–6), 831–839. https://doi.org/10.1016/S0146-6380(86)80020-1.

Katz, B.J., 1995. The green river shale: an eocene carbonate lacustrine source rock. Petroleum Source Rocks 310–324. https://doi.org/10.1007/978-3-642-78911-3_16.

Köster, J., van Kaam-Peters, H., Koopmans, M.P., et al., 1997. Sulphurisation of homohopanoids: effects on carbon number distribution, speciation, and 22S/22R epimer ratios. Geochem. Cosmochim. Acta 61, 2431–2452. https://doi.org/10.1016/s0016-7037(97)00110-5.

Lindner, A.W., 1983. Geology and geochemistry of some Queensland Tertiary oil shales. In: Miknis, F.P., McKay, J.F. (Eds.), Geochemistry and Chemistry of Oil Shales. American Chemical Society, Washington, pp. 97–118.

Liu, B., Bechtel, Achim, Sachsenhofer, Reinhard F., et al., 2017. Depositional environment of oil shale within the second member of permian Lucaogou formation in the Santanghu basin, Northwest China. Int. J. Coal Geol. 175, 10–25. https://doi.org/10.1016/j.coal.2017.03.011.

Liu, S.J., Gao, G., Jun, J., et al., 2022. Source rock with high abundance of C_{28} regular sterane in typical brackish-saline lacustrine sediments: biogenic source, depositional environment and hydrocarbon generation potential in Junggar Basin, China. J. Petrol. Sci. Eng. 208, 109670. https://doi.org/10.1016/j.petrol.2021.109670. Part D.

Lu, S.F., 2008. Petroleum Geochemistry [M]. Petroleum Industry Press (In Chinese).

Luo, Q.Y., Gong, L., Qu, Y., et al., 2018. The tight oil potential of the Lucaogou Formation from the southern Junggar Basin, China. Fuel 234, 858–871. https://doi.org/10.1016/j.fuel.2018.07.002.

Mahlstedt, N., Horsfield, B., Dieckmann, V., 2008. Second order reactions as a prelude to gas generation at high maturity. Org. Geochem. 39 (8), 1125–1129. https://doi.org/10.1016/j.orggeochem.2008.04.011.

Mello, M.R., Telnaes, N., Gaglianone, P.C., et al., 1988. Organic geochemical characterization of depositional environments of source rocks and oils in Brazilian marginal basins. Org. Geochem. 13 (1–3), 31–45. https://doi.org/10.1016/0146-6380(88)90023-X.

Moldowan, J.M., 1985. Organic geochemistry division of the geochemical society: alfred e. treibs award introduction of wolfgang k. scifert for the alfred e. treibs

award 1984. Geochem. Cosmochim. Acta 49 (7), 1671–1672. https://doi.org/10.1016/0016-7037(85)90276-5.
Pepper, A.S., Corvi, P.J., 1995. Simple kinetic models of petroleum formation. PartI: oil and gas generation from kerogen. Mar. Petrol. Geol. 12 (3), 291–319. https://doi.org/10.1016/0264-8172(95)98381-E.
Peters, K.E., Cassa, M.R., 1994. Applied source rock geochemistry. In: Magoon, L.B., Dow, W.G. (Eds.), The Petroleum System – from Source to Trap. American Association of Petroleum Geologists, Tulsa, OK, 3–117.
Peters, K.E., 1986. Guidelines for evaluating petroleum source rock using programmed pyrolysis. Am. Assoc. Petrol. Geol. Bull. 70, 318–329. https://doi.org/10.1306/94885688-1704-11D7-8645000102C1865D.
Peters, K.E., Moldowan, J.M., 1993. The Biomarker Guide: Interpreting Molecular Fossils in Petroleum and Ancient Sediments. Prentice–Hall, Englewood Cliffs, N. J https://doi.org/.
Peters, K.E., Walters, C.C., Mankiewicz, P.J., 2006. Evaluation of kinetic uncertainty in numerical models of petroleum generation. AAPG (Am. Assoc. Pet. Geol.) Bull. 90 (3), 387–403. https://doi.org/10.1306/10140505122.
Peters, K.E., Walters, C.C., Moldowan, J.M., 2005. The biomarker guide. In: Biomarkers and Isotopes in Petroleum Systems and Earth History (II), second ed. University Press, Cambridge.
Petersen, H.I., Rosenberg, P., 2000. The relationship between the composition and rank of humic coals and their activation energy distributions for the generation of bulk petroleum. Petrol. Geosci. 6 (2), 137–149. https://doi.org/10.1144/petgeo.6.2.137.
Pickel, W., Kus, J., Flores, D., et al., 2017. Classification of liptinite – ICCP system 1994. Int. J. Coal Geol. 169, 40–61. https://doi.org/10.1016/j.coal.2016.11.004.
Powell, T.G., McKirdy, D.M., 1973. Relationship between ratio of pristane to phytane, crude oil composition and geological environment in Australia. Nature 243, 37–39.
Prauss, M., Ligouis, B., Luterbacher, H., 1991. Organic matter and palynomorphs in the'Posidonienschiefer' (Toarcian, lower Jurassic) of southern Germany. In: Tyson, R.V., Pearson, T.H. (Eds.), Modern and Ancient Continental Shelf Anoxia 58. Geological Society Special Publication, pp. 335–351.
Quigley, T.M., Mackenzie, A.S., 1988. The temperature of oil and gas-formation in the sub-surface. Nature 333 (6173), 549–552. https://doi.org/10.1038/333549a0.
Rahman, H.M., Kennedy, M., Löhr, S., et al., 2017. Clay-organic association as a control on hydrocarbon generation in shale. Org. Geochem. 105, 42–55. https://doi.org/10.1016/j.orggeochem.2017.01.011.
Romero-Sarmiento, M.F., Euzen, T., Rohais, S., et al., 2016. Artificial thermal maturation of source rocks at different thermal maturity levels: application to the Triassic Montney and Doig formations in the Western Canada Sedimentary Basin. Org. Geochem. 97, 148–162. https://doi.org/10.1016/j.orggeochem.2016.05.002.
Rullkotter, J., Leythaeuser, D., Horsfield, B., et al., 1987. Organic matter maturation under the influence of a deep intrusive heat source: a natural experiment for quantitation of hydrocarbon generation and expulsion from a petroleum source rock (Toarcian Shale, northern Germany). In: Mattavelli, L., Novelli, L. (Eds.), Advances in Organic Geochemistry, Organic Geochemistry, vol. 13, pp. 847–856.
Saxby, J.D., 1980. Organic geochemistry of oil shales. In: Cook, A.C., Kantsler, A.J. (Eds.), Oil Shale Petrology Workshop. Wollongong, Australia, pp. 63–69.
Schaefer, R.G., Schenk, H.J., Hardelauf, H., et al., 1990. Determination of gross kinetic parameters for petroleum formation from Jurassic source rocks of different maturity levels by means of laboratory experiments. Org. Geochem. 16 (1–3), 115–120. https://doi.org/10.1016/0146-6380(90)90031-T.
Schenk, H.J., di Primio, R., Horsfield, B., 1997. The conversion of oil into gas in petroleum reservoirs. Part I. Comparative kinetic investigation of gas generation from crude oils of lacustrine, marine and fluviodeltaic origin by programmed-temperature closed-system pyrolysis. Org. Geochem. 26 (7), 467–481. https://doi.org/10.1016/S0146-6380(97)00024-7.
Schenk, H.J., Horsfield, B., 1998. Using natural maturation series to evaluate the utility of parallel reaction kinetics models: an investigation of Toarcian shales and Carboniferous coals, Germany. Org. Geochem. 29 (1–3), 137–154. https://doi.org/10.1016/S0146-6380(98)00139-9.
Seifert, W.K., Moldowan, J.M., 1986. Use of biological markers in petroleum exploration. In: Johns, R.B. (Ed.), Methods Geochem. Geophys. 24, 261–290.
Shanmugam, G., 1985. Significance of coniferous rain forests and related organic matter in generating commercial quantities of oil, Gippsland Basin, Australia. AAPG Bull. 69, 1241–1254. https://doi.org/10.1306/AD462BC3-16F7-11D7-8645000102C1865D.
Sherwood, N., 1991. Oil Shales. Department of Geology, University of Wollongong.
Tegelaar, E.W., Noble, R.A., 1994. Kinetics of hydrocarbon generation as a function of the molecular structure of kerogen as revealed by pyrolysis-gas chromatography. Org. Geochem. 22 (3–5), 543–574. https://doi.org/10.1016/0146-6380(94)90125-2.
ten Haven, H., de Leeuw, J., Peakman, T., et al., 1986. Anomalies in steroid and hopanoid maturity indices. Geochem. Cosmochim. Acta 50, 853–855. https://doi.org/10.1016/0016-7037(86)90361-3.
Ten Haven, H.L., De Leeuw, J.W., Rullkotter, J., et al., 1988. Application of biological markers in the recognition of paleohypersaline environments. In: Fleet, A.J., Kelts, K., Talbot, M.R. (Eds.), Lacustrine Petroleum Source Rocks. Geological Society Special Publication, pp. 3–26.
ten Haven, H.L., de Leeuw, J.W., Schenck, P.A., 1985. Organic geochemical studies of a Messinian evaporitic basin, northern Apennines (Italy) I: hydrocarbon biological markers for a hypersaline environment. Geochem. Cosmochim. Acta 49, 2181–2191. https://doi.org/10.1016/0016-7037(85)90075-4.
Tissot, B., Deroo, G., Hood, A., 1978. Geochemical study of the Uinta basin: formation of petroleum from the green River Formation. Geochem. Cosmochim. Acta 42 (10), 1459–1485. https://doi.org/10.1016/0016-7037(78)90018-2.
Tissot, B.P., Pelet, R., Ungerer, P.H., 1987. Thermal history of sedimentary basins, maturation indices, and kinetics of oil and gas generation. AAPG (Am. Assoc. Pet. Geol.) Bull. 71 (12), 1445–1466. https://doi.org/10.2310/6620.2008.08038.
Tissot, B.P., Welte, D.H., 1984. Petroleum Formation and Occurrence, second ed. SpringerVerlag, Heidelberg.
Volkman, J.K., Maxwell, J.R., 1986. Acyclic isoprenoids as biological markers. In: Johns, R.B. (Ed.), Biological Markers in the Sedimentary Record. Elsevier, Amsterdam, pp. 1–42.
Wang, M., Lu, S.F., Dong, Q., et al., 2011. Comparison on hydrocarbon generation kinetic models. J. China Univ. Petroleum (Edition of Natural Science) 35 (3), 12–18. https://doi.org/10.3969/j.issn.1673-5005.2011.03.003.
Yi, Zejun, 2018. Permian Geological Architecture and Formation Mechanism of Eastern Junggar Basin. China University of Geosciences (Beijing), Beijing (in Chinese).
Zumberge, J.E., 1984. Source rocks of the La Luna (upper cretaceous) in the middle Magdalena valley, Colombia, Palacas. In: Palacas, J.G. (Ed.), Geochemistry and Source Rock Potential of Carbonate Rocks. American Association of Petroleum Geologists, Studies in Geology, vol. 18, pp. 127–133.